

RESEARCH ARTICLE

10.1029/2021JD034689

Key Points:

- Measured vertical profiles of HONO near Los Angeles in May 2010 suggest a heterogeneous HONO source at the ground
- A new 1D chemistry and transport model that includes HONO formation on the ground reproduces the HONO concentration profiles
- The main daytime HONO source is adsorbed nitric acid/nitrate photolysis, followed by photo-enhanced NO₂ conversion

Correspondence to:

J. Stutz and J. L. Thomas,
jochen@atmos.ucla.edu;
jennie.thomas@univ-grenoble-alpes.fr

Citation:

Tuite, K., Thomas, J. L., Veres, P. R., Roberts, J. M., Stevens, P. S., Griffith, S. M., et al. (2021). Quantifying nitrous acid formation mechanisms using measured vertical profiles during the CalNex 2010 campaign and 1D column modeling. *Journal of Geophysical Research: Atmospheres*, 126, e2021JD034689. <https://doi.org/10.1029/2021JD034689>

Received 29 JAN 2021

Accepted 3 JUN 2021

Author Contributions:

Conceptualization: Katie Tuite, Jennie L. Thomas, Olga Pikelnaya, Jochen Stutz

Data curation: Patrick R. Veres, James M. Roberts, Philip S. Stevens, Stephen M. Griffith, Sebastien Dusanter, James H. Flynn, Louisa Emmons, Si-Wan Kim, Rebecca Washenfelder, Cora Young, Catalina Tsai, Olga Pikelnaya, Jochen Stutz










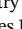

Formal analysis: Katie Tuite, Jennie L. Thomas, Shaddy Ahmed, Catalina Tsai, Jochen Stutz

Funding acquisition: James M. Roberts, Jochen Stutz

Investigation: Katie Tuite, Patrick R. Veres

Methodology: Katie Tuite, Jennie L. Thomas, Patrick R. Veres, Shaddy Ahmed, Catalina Tsai, Olga Pikelnaya, Jochen Stutz

Quantifying Nitrous Acid Formation Mechanisms Using Measured Vertical Profiles During the CalNex 2010 Campaign and 1D Column Modeling

Katie Tuite¹, Jennie L. Thomas² , Patrick R. Veres³ , James M. Roberts³ , Philip S. Stevens⁴ , Stephen M. Griffith⁵ , Sebastien Dusanter⁶, James H. Flynn⁷, Shaddy Ahmed² , Louisa Emmons⁸ , Si-Wan Kim⁹ , Rebecca Washenfelder³ , Cora Young¹⁰ , Catalina Tsai¹¹, Olga Pikelnaya¹¹, and Jochen Stutz¹ 

¹Department of Atmospheric and Oceanic Sciences, University of California Los Angeles, Los Angeles, CA, USA,

²Institut des Géosciences de l'Environnement, Université Grenoble Alpes, CNRS, IRD, Grenoble INP, Grenoble,

France, ³Earth Systems Research Laboratory, National Oceanic and Atmospheric Administration, Boulder, CO, USA,

⁴School of Public and Environmental Affairs and Department of Chemistry, Indiana University, Bloomington, IN,

USA, ⁵Department of Atmospheric Sciences, National Central University, Taoyuan, Taiwan, ⁶Département Sciences de

l'Atmosphère et Génie de l'Environnement, IMT Lille Douai, Université de Lille, Lille, France, ⁷Department of Earth

and Atmospheric Sciences, University of Houston, Houston, TX, USA, ⁸Atmospheric Chemistry Observations and

Modeling Lab, National Center for Atmospheric Research, Boulder, CO, USA, ⁹Department of Atmospheric Sciences,

Yonsei University, Seoul, Korea, ¹⁰Department of Chemistry, York University, Ontario, Canada, ¹¹South Coast Air

Quality Management District, Diamond Bar, CA, USA

Abstract Nitrous acid (HONO) is an important radical precursor that can impact secondary pollutant levels, especially in urban environments. Due to uncertainties in its heterogeneous formation mechanisms, models often under predict HONO concentrations. A number of heterogeneous sources at the ground have been proposed but there is no consensus about which play a significant role in the urban boundary layer. We present a new one-dimensional chemistry and transport model which performs surface chemistry based on molecular collisions and chemical conversion, allowing us to add detailed HONO formation chemistry at the ground. We conducted model runs for the 2010 CalNex campaign, finding good agreement with observations for key species such as O₃, NO_x, and HO_x. With the ground sources implemented, the model captures the diurnal and vertical profile of the HONO observations. Primary HO_x production from HONO photolysis is 2–3 times more important than O₃ or HCHO photolysis at mid-day, below 10 m. The HONO concentration, and its contribution to HO_x, decreases quickly with altitude. Heterogeneous chemistry at the ground provided a HONO source of 2.5×10^{11} molecules cm⁻² s⁻¹ during the day and 5×10^{10} molecules cm⁻² s⁻¹ at night. The night time source was dominated by NO₂ hydrolysis. During the day, photolysis of surface HNO₃/nitrate contributed 45%–60% and photo-enhanced conversion of NO₂ contributed 20%–45%. Sensitivity studies addressing the uncertainties in both photolytic mechanisms show that, while the relative contribution of either source can vary, HNO₃/nitrate is required to produce a surface HONO source that is strong enough to explain observations.

1. Introduction

Nitrous acid (HONO) chemistry in the polluted boundary layer has been an area of research for nearly five decades. It is well established that HONO photolysis (R1) is an important source of hydroxyl radicals (OH) throughout the day, contributing up to 55% of the primary OH formation (Alicke et al., 2002, 2003; Dusanter et al., 2009; Elshorbany et al., 2009; Kleffmann, 2007; Kleffmann et al., 2005; Mao et al., 2010; Ren et al., 2003; Volkamer et al., 2010; Young et al., 2012).



Although it has a large impact on the oxidative capacity of the atmosphere, HONO chemistry is often excluded from or simplified in 3D air quality models due to uncertainties in its formation mechanisms. This leads to an underestimation of HONO, which consequently impacts predicted concentrations of radicals

Project Administration: Jochen Stutz

Resources: Philip S. Stevens, Jochen Stutz

Software: Katie Tuite, Jennie L. Thomas, Shaddy Ahmed, Louisa Emmons, Si-Wan Kim, Catalina Tsai, Olga Pikelnaya, Jochen Stutz

Supervision: Jennie L. Thomas, Jochen Stutz

Validation: Patrick R. Veres, James M. Roberts, Rebecca Washenfelder, Cora Young, Catalina Tsai, Olga Pikelnaya

Visualization: Katie Tuite, Jennie L. Thomas

Writing – original draft: Katie Tuite, Jennie L. Thomas, Jochen Stutz

Writing – review & editing: Katie Tuite, Jennie L. Thomas, Patrick R. Veres, James M. Roberts, Philip S. Stevens, Sebastien Dusanter, James H. Flynn, Shaddy Ahmed, Louisa Emmons, Si-Wan Kim, Rebecca Washenfelder, Cora Young, Catalina Tsai, Olga Pikelnaya, Jochen Stutz

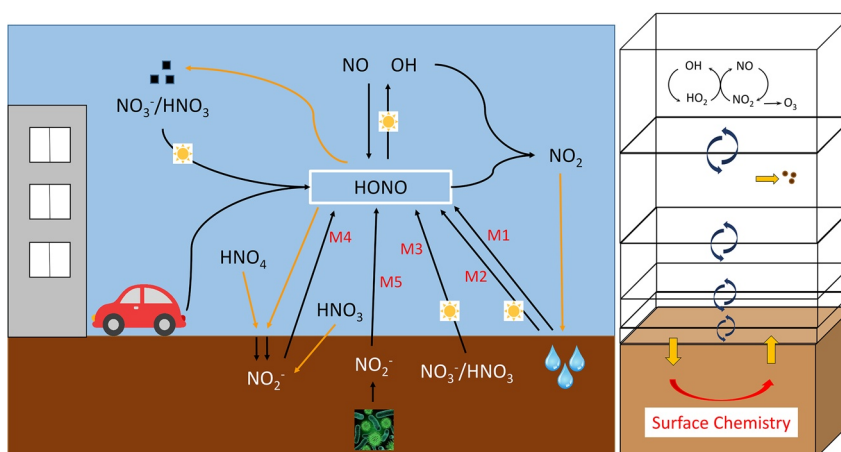


Figure 1. The cartoon on the left shows common HONO sources and sinks, with heterogeneous processes labeled M1–M5 in red. On the right is an example model grid schematic showing the interaction between gas phase chemistry, surface chemistry, vertical mixing, and aerosol uptake.

and secondary pollutants like ozone (Czader et al., 2012; Elshorbany et al., 2012). Developing accurate HONO source representation is necessary to improve air quality modeling, which is increasingly important as air quality standards become more strict (Sarwar et al., 2008).

HONO chemistry includes homogeneous and heterogeneous reactions, biological processes in soil, and direct emission from combustion sources (Figure 1). The main gas phase reactions include loss via photolysis (R1) and reaction with OH (R2), and production through the NO + OH reaction (R3).



Measured diurnal profiles show that HONO concentrations accumulate throughout the night and drop off in the early morning once photolysis becomes active. Nocturnal surface levels can reach up to several ppb in urban regions (Kleffmann et al., 2006; Stutz et al., 2010; Wong et al., 2011), while daytime levels have been reported up to a few hundred ppt (Acker et al., 2006; Kleffmann et al., 2005; Wong et al., 2012; Zhou et al., 2007). A strong HONO source is required to maintain these levels, particularly during the day when the HONO lifetime is only 10–20 min.

Pseudo-steady state (PSS) calculations and models show that HONO levels are greatly underestimated when only homogeneous chemistry (R1–R3) is considered (Czader et al., 2012; Kleffmann, 2007; Kleffmann et al., 2005; Li et al., 2011; Sarwar et al., 2008; Tsai et al., 2018; Zhou et al., 2002). HONO is directly emitted by anthropogenic combustion processes, but this is less than 1% of NO_x emissions (Kirchstetter et al., 1996; Kramer et al., 2019; Kurtenbach et al., 2001; Neuman et al., 2016) and cannot explain atmospheric levels by itself. Measured vertical profiles show HONO concentrations are greatest near the ground (Kleffmann et al., 2003; VandenBoer et al., 2013; Villena et al., 2011; Wong et al., 2011, 2012), indicating that a surface source is likely. Multiple heterogeneous formation mechanisms have therefore been proposed to explain this missing HONO source.

1.1. Heterogeneous HONO Chemistry

Laboratory studies have found that HONO is produced from NO₂ conversion on humid surfaces (mechanism M1 in Figure 1), following a reaction mechanism (R4) which is first order with respect to both NO₂ and water vapor (Jenkin et al., 1988; Lammel & Cape, 1996; Pitts et al., 1984; Sakamaki et al., 1983; Svensson et al., 1987).



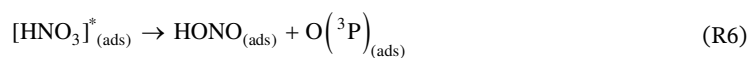
There is significant evidence that this reaction is the main source of nocturnal HONO and allows for an accurate description of HONO and HONO/NO₂ ratios at night (Alicke et al., 2003; Kleffmann et al., 2003; VandenBoer et al., 2013; Wong et al., 2011). While R4 occurs during the day as well, it does not produce HONO at the rate needed to sustain daytime levels and many studies have shown evidence that a photolytic source is required (Acker et al., 2006; Alicke et al., 2002; Kleffmann et al., 2005; Wong et al., 2012).

Photo-enhanced heterogeneous conversion of NO₂ to HONO (M2 in Figure 1) has been found to occur on a variety of surfaces, including soot (Ammann et al., 1998; Aubin & Abbatt, 2007; Khalizov et al., 2010; Monge et al., 2010), humic acid (Bartels-Rausch et al., 2010; Stemmler et al., 2006, 2007), and organic films (Brigante et al., 2008; George et al., 2005; Gutzwiller et al., 2002). A mechanism proposed by Stemmler et al. (2006) suggests HONO formation from NO₂ conversion on humic acid surfaces is first order in NO₂ and linearly dependent on irradiance and surface area (SA).

$$P_{\text{HONO}} \propto \text{SA} \times [\text{NO}_2] \times \text{irradiance} \quad (1)$$

Wong et al. (2013) included a sunlight dependent NO₂ to HONO reactive uptake coefficient (γ) in their 1D model study and found good agreement between modeled and observed HONO levels during the 2009 SHARP field campaign in Texas. Without this parameterization, daytime HONO levels were underestimated by at least 50%. Other studies also suggest this conversion provides a major daytime source, showing that HONO correlates with NO₂ levels and/or NO₂ photolysis rates (Laufs et al., 2017; Tsai et al., 2018; Vogel et al., 2003).

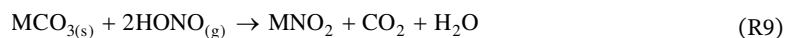
Another daytime HONO source is the photolysis of surface adsorbed HNO₃/nitrate (M3 in Figure 1), which proceeds at a rate 1–4 orders of magnitude faster than gas phase or aqueous HNO₃ photolysis (Baergen & Donaldson, 2013, 2016; Ramazan et al., 2004; Ye et al., 2016, 2019; Zhou et al., 2002, 2003). R5–R8 describes the mechanism proposed by Zhou et al. (2002). NO₂ in R7 is the dominant product over R6 in the actinic region of solar radiation.



The HONO produced in R6 and R8 can desorb from the surface into the gas phase. This mechanism has been shown to be important in low NO_x forested environments (Zhang et al., 2012; Zhou et al., 2011). Although photo-enhanced conversion of NO₂ is often thought to be the dominant HONO formation pathway in high NO_x areas, HNO₃ photolysis has also been confirmed as a significant source in the urban regions near Philadelphia (Sarwar et al., 2008) and Houston (Karamchandani et al., 2014). Enhanced photolysis has been shown to occur on glass (Ye et al., 2019; Zhou et al., 2002), building materials (Ye et al., 2016), and urban grime (Baergen & Donaldson, 2013, 2016), indicating that this mechanism likely plays a role in urban HONO production.

Both of these proposed photolytic mechanisms can occur on aerosols in addition to the ground. Due to the much smaller surface area available on aerosols and deactivation of reactive sites during aging, the aerosol source is thought to be minor in comparison in typical settings (Kalberer et al., 1999; Kleffmann et al., 2003; Stemmler et al., 2007; Vogel et al., 2003).

A recent HONO source proposed by VandenBoer et al. (2015) is the displacement of surface nitrite by strong atmospheric acids like HCl and HNO₃ (M4 in Figure 1). Throughout the night, the primary HONO sink is deposition to the surface, where it can react with carbonate material to form nitrite.



VandenBoer et al. (2013) suggests that this nocturnally deposited HONO may form a surface reservoir that can be released the following day. Laboratory studies find that HCl and HNO₃ can displace surface nitrite with an efficiency of 1%–20%. Using the mean value of 9%, VandenBoer et al. (2015) showed that this mechanism contributed up to 23% of the total noontime HONO flux in Bakersfield, California during the CalNex campaign.

Biological processes in soil provide another potential atmospheric HONO source (M5 in Figure 1) (Maljanen et al., 2013; Meusel et al., 2018; Oswald et al., 2013; Scharcko et al., 2015; Su et al., 2011). Nitrification and denitrification produce nitrite, which undergoes acid-base reactions and partitioning between air and the aqueous phase in soil.



R10 depends on the pH and NO₂⁻ concentration of the soil. Oswald et al. (2013) performed laboratory studies to compare emissions of HONO and NO from soils from a variety of ecosystems. They found that HONO can account for up to 50% of the total reactive nitrogen released from soil, especially in arid and arable soils with water content below 20% water holding capacity.

1.2. Linking Surface Chemistry to Atmospheric Measurements

A challenge in studying the link between chemical transformations on the ground and the chemistry in the overlying atmosphere is the role of vertical transport to and from the surface. This was illustrated by 1D modeling studies by Geyer and Stutz (2004a) and (2004b), who showed that concentrations change on the scale of one meter or less near the surface. Similar conclusions were derived by nighttime and daytime HONO modeling studies (Tsai et al., 2018; Wong et al., 2011, 2013), which all showed a strong concentration gradient near the surface. Another challenge for modeling studies of atmospheric HONO is the poorly known surface (ground) formation chemistry. To address this issue, flexibility in the model setup and the ability to perform sensitivity studies are essential.

One-dimensional chemistry and transport models are an ideal tool to study poorly constrained surface chemistry. A number of 1D models have provided valuable insight into similar atmospheric systems, such as the interaction of snow with the atmosphere (Cao et al., 2014, 2016; Thomas et al., 2011, 2012; Toyota et al., 2014; Wang et al., 2020), forest canopies (Boy et al., 2011), and the marine boundary layer (von Glasow et al., 2002a, 2002b). However, only few studies have addressed the surface chemistry of HONO (Karamchandani et al., 2014; Tsai et al., 2018; Wong et al., 2011, 2013). To investigate this specific surface-atmosphere chemical system, we present a newly developed 1D model, the Platform for Atmospheric Chemistry and vertical Transport in one dimension (PACT-1D). PACT-1D is based on the success of our previous modeling (Tsai et al., 2018; Wong et al., 2011, 2013), and includes improved capability to perform mechanistic and sensitivity studies of these systems.

In this paper we analyze observed vertical concentration profiles of HONO, NO₂, and other compounds during the 2010 CalNex field experiment (Section 2) using PACT-1D (Section 3). We use PACT-1D to test if HONO surface formation can reproduce the observations, and explore the contribution of the mechanisms (Section 4).

2. Measurements

The 2010 CalNex experiment took place in Pasadena, CA from mid-May to mid-June 2010 (Ryerson et al., 2013). The ground-site was located on the California Institute of Technology (Caltech) campus with in-situ measurements collected near the surface at altitudes between 3 m and 10 m and remote sensing

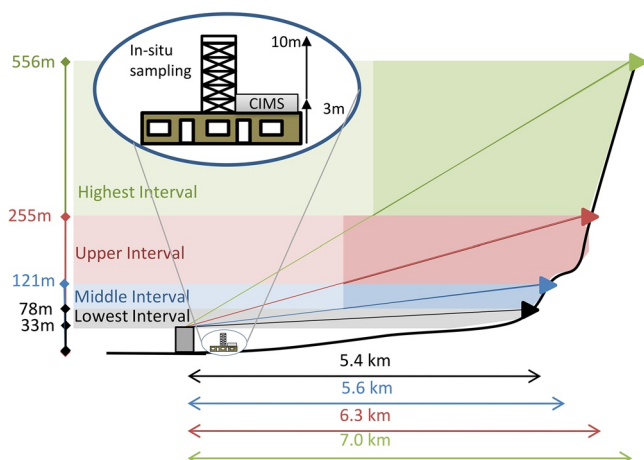


Figure 2. Sketch of the LP-DOAS field setup during the CalNex 2010 experiment.

observations on top of Caltech's library at ~35 m agl. All CalNex observations are publicly available at www.esrl.noaa.gov/csd/projects/calnex/.

In this study we focus on observations relevant for understanding the formation of HONO and its impact on atmospheric chemistry. We use HONO data from two instruments: UCLA's long-path Differential Optical Absorption Spectroscopy instrument (LP-DOAS) and NOAA's Chemical Mass Spectrometer (CIMS). NOAA's CIMS sampled air at 3 m agl, while the LP-DOAS probed air between 33 m agl and 556 m agl in four different altitude intervals. All other in-situ measurements used here were sampled at 10 m agl on top of a scaffolding tower.

We concentrate on a four day period, May 26–30, 2010, during which a variety of conditions were encountered, including cloudy days and the highest ozone levels of the experiment. This period also has the best coverage of all instruments, in particular the LP-DOAS instrument.

2.1. LP-DOAS

The setup of the LP-DOAS during CalNex, as well as the data retrieval techniques, have been described previously (Tsai et al., 2014; Wong et al., 2011, 2012), therefore we will only briefly describe them here. Figure 2 shows a schematic of the site setup. The LP-DOAS consists of a main telescope/spectrometer unit, which was located on top of Millikan Library on the Caltech campus at 33 m altitude. Four arrays of retroreflectors were mounted on a nearby mountain at different distances and altitudes. We refer to these retroreflectors and the associated air samples by their relative altitudes: lower (78 m), middle (121 m), high (255 m), highest (556 m). The instrument was aimed at the four reflectors using a cycle of measurements with a repeat interval of 15–30 min, depending on visibility. The light received back was measured in the 300–380 nm range with a spectral resolution of 0.6 nm. Trace gas path-averaged concentrations were retrieved using established DOAS techniques as described in Platt and Stutz (2008). Average detection limits for NO₂ and HONO on a single absorption path were 0.16 and 0.06 ppb, respectively. It should also be pointed out that the LP-DOAS, which was located around 550 m southeast of the other instruments, averaged over ~5–7 km absorption light paths.

The LP-DOAS measured continuously throughout CalNex, however, low visibility and low clouds blocked the light beams at some times. Low clouds were especially common during the night and often only the lowest light path data was available. The dates chosen for this modeling study had good coverage along all light paths. Vertical profiles from LP-DOAS measurements were constructed following the method described in Tsai et al. (2014). Briefly, the path-averaged mixing ratios were first linearly interpolated onto the time grid of the lowest light path and then converted to height interval-average mixing ratios. These averages are reported at the midpoint of each height interval (55.5, 99.5, 188, and 405.5 m).

2.2. NI-PT-CIMS

A negative-ion proton-transfer chemical ionization mass spectrometer (NI-PT-CIMS) using acetate ions provided HONO and HNO₃ observations at 1-min resolution during CalNex and has been described previously (Roberts et al., 2010; Veres et al., 2011). Briefly, ambient air was sampled through a 1.5 m PTFE inlet heated from a point approximately 3 m agl. Acidic molecules are ionized via proton abstraction reactions with acetate ions (CH₃COO⁻) and detected, as the conjugate anion, using a quadrupole mass spectrometer. Instrument backgrounds using a sodium carbonate denuder were performed every 190 min for 30 min.

HONO calibrations were performed in-field approximately every two days using a portable source described elsewhere (Roberts et al., 2010). Measurement of HONO by the NI-PT-CIMS required correction for NO₂. Correction factors were determined through laboratory additions of NO₂ as a function of relative humidity with NO₂ quantified by CRDS. Detection limits for HONO were 10 ppt, with an uncertainty of 30% + 20 ppt for 1-min measurements. Nitric acid calibrations were performed during post-field laboratory work using a

Table 1
Overview of CalNex Measurements Used in This Study

Species/parameter	Instrument	Operator	References
O ₃	UV-absorption	Univ. Houston (UH)	
NO/NO ₂	Chemiluminescence with photolytic converter	Univ. Houston (UH)	Pollack et al. (2010)
NO ₂	Cavity Ring-Down Spectroscopy (CRDS)	NOAA	Washenfelder et al. (2011)
OH/HO ₂	Laser Induced Fluorescence (LIF-FAGE)	Indiana Univ.	Dusanter et al. (2009) and Griffith et al. (2016)
VOC	GC-MS	NOAA	Borbon et al. (2013) and Gilman et al. (2010)
Actinic flux	Spectroradiometer	Univ. Houston (UH)	Shetter and Müller (1999)
Aerosol number distribution	TSI SMPS	CU Boulder	Hayes et al. (2013)
HONO, HNO ₃	CIMS	NOAA	Veres et al. (2008)

permeation source calibrated using UV optical absorption (Neuman et al., 2003). HNO₃ was measured with a detection limit of 15 ppt, with a stated uncertainty of 30% + 30 ppt for 1-min measurements.

2.3. Other Measurements

We use a number of other observations from CalNex in our analysis and model evaluation. Table 1 lists these parameters, the respective instruments, and literature references of the CalNex results.

3. The Platform for Atmospheric Chemistry and Vertical Transport in One Dimension (PACT-1D)

3.1. Model Description

In this study we describe and use a new vertical column model, the Platform for Atmospheric Chemistry and vertical Transport in one dimension (PACT-1D). The new model is similar to past vertical column models used to study the interactions between chemical processing and vertical transport processes, where chemistry is calculated online and dynamics and physics are provided as input (Geyer & Stutz, 2004a). PACT-1D solves both 1D transport and chemical kinetics resulting in the time evolution (t) of a chemical species (i) at altitude (z). The continuity equation for the change in concentration C for the 1D chemical system is given by Equation 2.

$$\frac{dC_{(i,t,z)}}{dt} = P_{(i,t,z)} - L_{(i,t,z)} + F_{(i,t,z)} + E_{(i,t,z)} \quad (2)$$

P and L represent chemical production and loss, F refers to the flux in/out of the box due to vertical mixing, including loss to the ground (deposition), and E is the rate of emissions. We treat each process including chemistry, vertical mixing, and emissions as separable using operator splitting.

Emissions are provided as input and are time and height dependent. Chemical production and loss are described using the Regional Atmospheric Chemistry Mechanism version 2 (RACM2) (Goliff et al., 2013), implemented with the Kinetics Pre-Processor (Sandu & Sander, 2006). Photolysis rates are provided as input. In addition to the RACM2 gas phase chemistry, we include non-reactive uptake of gases to aerosols and heterogeneous surface reactions on aerosols. For heterogeneous chemistry, the aerosol surface area (S) is prescribed in each model level (z) at a given time (t) according to

$$S_{(z,t)} = 4\pi r_{(z,t)}^2 N_{(z,t)} \quad (3)$$

where r and N represent the radius and number concentration of a mono-disperse aerosol that best represents the surface area available for reactions. Aerosol physical properties (N and r) are given as model input. Therefore, no aerosol physics is calculated online within the model. Irreversible uptake to and heterogeneous reactions on aerosols are treated with the rate constant (k_r) given by

$$k_T = \frac{1}{4} \nu S \gamma J \quad (4)$$

where ν is the mean molecular speed, S is the aerosol surface area, and γ represents the probability of irreversible uptake or interfacial reaction. The flux of molecules to the aerosol surface in the transition regime, J , is calculated according to Fuchs and Sutugin (1971). This corrects the rate of diffusion for gas molecules toward an aerosol surface when the particle size is similar to the mean free path in air, the so called *transition regime*.

Vertical mixing and loss to the ground are solved together in the vertical mixing term, given as $F_{(i,t,z)}$ in Equation 2. We treat vertical mixing and surface loss (i.e., deposition) for each species according to

$$\frac{\partial}{\partial t} \phi_{(i,t,z)} = \frac{1}{\rho_{(i,t,z)}} \frac{\partial}{\partial z} \left(\rho_{(i,t,z)} K_{D(i,t,z)} \frac{\partial}{\partial z} \phi_{(i,t,z)} \right) + R_{(i,t)} \quad (5)$$

where ϕ_i is the species concentration in mixing ratio units, ρ is the air density, and R represents loss to the ground in the lowest model level. $K_{D(i,t,z)}$ is the sum of eddy diffusivity ($K_{(i,t,z)}$) plus molecular diffusion ($D_{(i,t,z)}$). To treat vertical mixing and loss to the ground, we discretize the model levels below 1 m using a log scale grid such that the lowest model level is appropriate for treatment of a laminar molecular diffusive layer in direct contact with the Earth's surface. $K_{(i,t,z)}$ decreases in a log profile toward the surface to a molecular diffusion coefficient in the lowest model level.

A unique feature of the model is that uptake and chemistry on the ground (R) are calculated using molecular collisions on the ground and applying an uptake probability (α) or reactive uptake coefficient (γ). We then solve Equation 5 numerically using the Crank-Nicolson method (Brasseur & Jacob, 2017), which is numerically stable for a variety of non-uniform grids and time steps.

Upon solving Equation 5, we calculate the deposition rate for each time step. This method allows for molecular level interaction with the surface, resulting in deposition without the need to prescribe a deposition velocity. We include interactive surface chemistry, which can lead to release of species from the ground into the gas phase. More details are provided in Section 3.3.

3.2. Model Setup for CalNex Campaign

PACT-1D was initialized using both model data (from WRF-Chem, MOZART, MEGAN, and CAMS) and observational data from the CalNex 2010 campaign (Table 1). The 24-h period from May 26, 2010 18:00 through May 27, 2010 17:00 was used as model spin up. The model subdivides the lowest 5,000 m of the atmosphere into 26 grid cells, with model grid box upper boundaries at: 1×10^{-3} , 0.01, 0.1, 1, 3, 6, 10, 20, 33, 50, 78, 90, 110, 121, 150, 175, 255, 300, 556, 750, 1,000, 1,500, 2,000, 3,000, 4,000, and 5,000 m. A 20 s chemical time step was used for each model run.

Time varying profiles of temperature, relative humidity, and pressure were extracted from a WRF-Chem model run for CalNex (Kim et al., 2016), which provided values above ~ 180 m. These were interpolated onto the 1D vertical grid and measured meteorological data was used to create a profile to the surface. Below 180 m, temperature was calculated based on 10 m measurements of wind speed and temperature, the measured boundary layer height, and atmospheric stability parameters. Relative humidity was given a constant value equal to the measurements at 10 m and pressure was calculated using the surface pressure and scale height. We take eddy diffusion coefficients (K_z) from WRF-Chem as well (Kim et al., 2016). These values start at ~ 50 m and a log interpolation was implemented to parameterize K_z values to the ground. The vertical mixing considered boundary layer height variation over the three day period, which is explicitly calculated via the planetary boundary layer (PBL) parameterization used within WRF-Chem.

Aerosol number concentration profiles were initialized using data from the TSI Scanning Mobility Particle Sizer (SMPS) instrument. Within the boundary layer, the number concentration was set equal to the measurements at 10 m and then decreased exponentially to one fifth of this value in the top layer of the model. The aerosol radius was assumed to be constant at 150 nm, following the study by Tsai et al. (2014).

Photolysis rates were initialized using the Tropospheric Ultraviolet-Visible (TUV) radiation model (v5.0) which was run for our test date and location. To account for clouds, measured NO₂ photolysis rates were used to scale the TUV values for all species.

Input anthropogenic emissions are based on the U.S. Environmental Protection Agency (EPA) National Emission Inventory (NEI) and the Fuel-based Inventory for motor Vehicle Emission (FIVE), which have been processed for use in WRF-Chem (Kim et al., 2016). Biogenic emissions are from the MEGAN model for May 2010. Anthropogenic NO_x emissions were emitted between 0.1 m and 1 m and VOC emissions were emitted between 0.1 m and 10 m. The emissions were scaled so that model concentrations matched those observed by the LP-DOAS and in-situ observations, using realistic emission injection altitudes for different emission source types. In some cases, the emissions are scaled by up to 50% in order to reproduce realistic VOC and NO_x concentrations, as well as NO₂ concentration profiles. Emissions scaling is needed to reproduce observations due to the fine model vertical resolution, which employs a much higher resolution grid vertically than typical 3D chemical transport models. 3D models quickly dilute these emissions into larger volumes of air resulting in lower concentrations of species that are directly emitted which impacts ozone chemistry and other non-linear atmospheric chemical cycling. In addition, the WRF-Chem emissions are general values for either weekday or weekend and have large uncertainties when modeling specific dates and events at high time resolution. This period includes the weekend (Saturday 5/29 and Sunday 5/30) before a major holiday (Memorial day).

Soil NO emissions are taken from the Copernicus Atmospheric Monitoring Service (CAMS) global and regional emissions dataset, which considers surface type, for May 2012 near Pasadena, CA (Granier et al., 2019; Simpson et al., 2014). Anthropogenic HONO emissions were included using an emission ratio of HONO/NO_x = 0.003 (Kurtenbach et al., 2001). A range of 0.003–0.008 is reported in literature (Kirchstetter et al., 1996; Kramer et al., 2019; Kurtenbach et al., 2001; Neuman et al., 2016) and due to the lower number of diesel engine vehicles in the United States compared to Europe where many of these studies were conducted, we chose a value at the lower end of this range.

To better simulate the urban atmosphere, chlorine chemistry and parameterized nitrate aerosol chemistry were added to the RACM2 mechanism. Aerosol nitrate is formed through uptake of HNO₃ and N₂O₅, with aerosol uptake coefficients of 0.1 and 0.02, respectively. Partitioning between gas phase HNO₃ and aerosol nitrate is based on the study by Guo et al. (2017), who found a campaign average partitioning ratio, $\epsilon(\text{NO}_3^-)$, of 39% for PM1 during CalNex.

$$\epsilon(\text{NO}_3^-) = \frac{\text{NO}_3^-}{\text{HNO}_3 + \text{NO}_3^-} \quad (6)$$

Similar to photolysis of HNO₃ on the ground, nitrate in aerosol can also photolyze to give HONO. This is added to the mechanism with a rate 45 times that of gas phase nitric acid (Karamchandani et al., 2014; Zhou et al., 2003).

3.3. Interactive Treatment of Surface Chemistry

The proposed HONO formation mechanisms occur at the ground, therefore we implemented detailed surface heterogeneous chemistry within PACT-1D. Deposition is calculated from the number of molecular collisions with the ground and an uptake coefficient, allowing for molecular level chemical conversions and surface emissions. The quantity of species available for reactions on the ground was initialized using a model spin-up of four days to achieve near steady state conditions. The HONO formation mechanisms described in Section 1.1 were added to PACT-1D with model implementation described below.

3.3.1. NO₂ Hydrolysis

Conversion of NO₂ to HONO on the ground is implemented into the model using reaction R4. NO₂ deposition is tracked and for every two molecules deposited, one HONO molecule is released from the surface

and one HNO₃ molecule is added to the surface storage term. The ground NO₂ uptake coefficient ($\gamma_{\text{NO}_2, \text{dark}}$) is set at 1×10^{-5} (Trick, 2004).

3.3.2. Photo-Enhanced NO₂ Conversion

The photo-enhanced conversion of NO₂ to HONO is included using the parameterization by Wong et al. (2013). In Wong et al. (2012) and Wong et al. (2013), daytime HONO concentrations in Houston, Texas correlated with solar irradiance and they determined that the reactive uptake coefficient for NO₂ could be parameterized with a cubic dependence on the NO₂ photolysis rate (Equation 7).

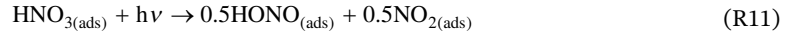
$$\gamma_{\text{NO}_2, \text{photo}} = 6 \times 10^{-5} \frac{J_{\text{NO}_2}^3}{J_{\text{NO}_2, \text{noon}}^3} \quad (7)$$

6×10^{-5} is the maximum reactive uptake coefficient. The average noontime photolysis rate for NO₂ ($J_{\text{NO}_2, \text{noon}}$) during the four days that we focused on (May 26–30, 2010) is $7 \times 10^{-3} \text{ s}^{-1}$. This photo-enhanced NO₂ uptake occurs in addition to dark uptake, giving an effective NO₂ deposition rate (V_{d, NO_2}) according to the following equation, where v is the mean molecular speed. V_{d, NO_2} drives NO₂ deposition in the model.

$$V_{d, \text{NO}_2} = \frac{1}{4} v \gamma_{\text{NO}_2, \text{dark}} + \frac{1}{4} v \gamma_{\text{NO}_2, \text{photo}} \quad (8)$$

3.3.3. Surface Nitric Acid/Nitrate Photolysis

Following the modeling study of Sarwar et al. (2008), we parameterize photolysis of surface adsorbed HNO₃ using the following reaction.



Surface HNO₃ is initialized in the model and its concentration is updated considering deposition and surface chemistry. HONO and NO₂ produced in R11 are released into the lowest model layer via desorption. HNO₃ deposition to the ground is calculated using an uptake coefficient of 0.1. The photolysis rate constant of this reaction ($J_{\text{HNO}_3, \text{surf}}$) is set to 45 times that of gas-phase HNO₃ (Karamchandani et al., 2014; Zhou et al., 2003), giving noon time values of $2.0 \times 10^{-5} \text{ s}^{-1}$ on May 27 and $2.5 \times 10^{-5} \text{ s}^{-1}$ on May 28 and 29. These rate constants are in accordance with the value of $2.5 \times 10^{-5} \text{ s}^{-1}$ reported by Zhou et al. (2003), and are also used for aerosol nitrate photolysis. The scaling factor of 45 is also consistent with that used by Fu et al. (2019) and Liu et al. (2021), who calculate $J_{\text{HNO}_3, \text{surf}}$ with the following equation.

$$J_{\text{HNO}_3, \text{surf}} = \frac{3.4 \times 10^{-5}}{7 \times 10^{-7}} J_{\text{HNO}_3} \quad (9)$$

3.4×10^{-5} is the median $J_{\text{HNO}_3, \text{surf}}$ reported by Ye et al. (2016) and 7×10^{-7} is the average noontime $J_{\text{HNO}_3, \text{gas}}$.

3.3.4. HONO Uptake, Nocturnal Storage, Acid Displacement

Uptake to the ground is an important loss for atmospheric HONO, especially at night. Once deposited, it forms surface nitrite through R9 and a similar reaction occurs with HNO₄. According to VandenBoer et al. (2015), this nitrite can be recycled back to gaseous HONO when displaced by a strong acid. In the model we assume that all HONO and HNO₄ deposited to the ground is converted to nitrite. Every HNO₃ molecule deposited then results in a HONO molecule emitted to the lowest model layer. The uptake coefficients for HONO, HNO₄, and HNO₃ are 1×10^{-4} , 0.01, and 0.1, respectively. To ensure there is a sufficient amount of nitrite present to be displaced, its concentration is tracked and if it falls below a monolayer ($\sim 1 \times 10^{13} \text{ molecules cm}^{-2}$), the HONO source is scaled by $\frac{[\text{NO}_2^-]}{1 \times 10^{13}}$.

3.3.5. Biogenic Emissions

Oswald et al. (2013) determined that HONO can contribute up to 50% of reactive nitrogen released from soil, comparable to soil NO emissions. Soil NO emissions are included in the model as input. We assume

Table 2
Overview of PACT-1D Model Runs

Model run	Description
NoSurf	HONO chemistry on the ground not included
Base	HONO chemistry on the ground included
Sens1	$\gamma_{\text{NO}_2, \text{max}}$ decreased by 50%, $J_{\text{HNO}_3, \text{surf}}$ increased by 25%
Sens2	$\gamma_{\text{NO}_2, \text{max}}$ increased by 2×, $J_{\text{HNO}_3, \text{surf}}$ decreased by 20%
Sens3	$\gamma_{\text{NO}_2, \text{max}}$ decreased by 90%, $J_{\text{HNO}_3, \text{surf}}$ increased by 60%
Sens4	$\gamma_{\text{NO}_2, \text{max}}$ increased by 5×, $J_{\text{HNO}_3, \text{surf}}$ decreased to gas phase J_{HNO_3}

that NO and HONO make up the majority of reactive nitrogen and therefore set HONO emissions equal to NO as an upper limit.

4. Results and Discussion

We use PACT-1D to simulate HONO levels during the CalNex campaign and analyze the importance of ground sources. An overview of each model run is provided in Table 2 and each is discussed below.

4.1. Model Run Without HONO Surface Chemistry (NoSurf Run)

A model run (NoSurf) was first performed to investigate HONO concentrations without ground surface chemistry. In this run, HONO was impacted by gas phase chemistry, direct emissions, deposition to the ground with an uptake coefficient of 1×10^{-4} , uptake on aerosol surfaces with an uptake coefficient of 1×10^{-3} , and formation from aerosol nitrate photolysis. HONO levels at 3 m were compared to the CIMS measurements (Figure 3, bottom right). Modeled HONO, shown in orange, remained around 0.1 ppb or lower during daytime periods. May 28 and 29 showed an early morning peak between 0.15 ppb and 0.3 ppb. Daytime and nighttime concentrations for all three days were significantly lower than observations, indicating that gas phase formation, direct emissions, and aerosol nitrate photolysis cannot completely explain HONO levels and that an additional source is required.

4.2. Model Results With Interactive Surface Chemistry (Base Run)

When heterogeneous HONO formation sources at the ground were implemented in PACT-1D (Base run), the model matched observations much better (Figure 3). The model captures the general trend and values of major species including NO_x , HO_x , and O_3 . Due to lack of horizontal advection in PACT-1D, however, there are some discrepancies related to changes in air mass, for example near midnight on May 30. The model also misses some of the afternoon NO_x peaks, which are due to advection of polluted air from downtown Los Angeles. These dates correspond to the start of the Memorial Day holiday weekend as well, making traffic emissions more difficult to estimate.

The overprediction of OH and underprediction of HO_2 in PACT-1D is consistent with results from Griffith et al. (2016) and is likely due to missing radical processes in the RACM2 mechanism. Griffith et al. (2016) suggests that reactivity between OH and saturated hydrocarbons and OH and aldehydes is under predicted in the mechanism which leads to an over prediction of OH and under prediction of HO_2 . Similar results were reported by Wolfe et al. (2016), who found that production of HO_2 from reactions of OH with HCHO, CO and other hydrocarbons was too slow in the RACM2 mechanism to accurately capture OH and HO_2 observations.

The diurnal HONO trend is captured in the Base run, showing mixing ratios increasing overnight, followed by a sharp decrease in the early morning. Concentrations are substantially higher compared to the NoSurf run, with daytime values ranging between 0.1 ppb and 0.5 ppb and night time values increasing to 1.2–1.6

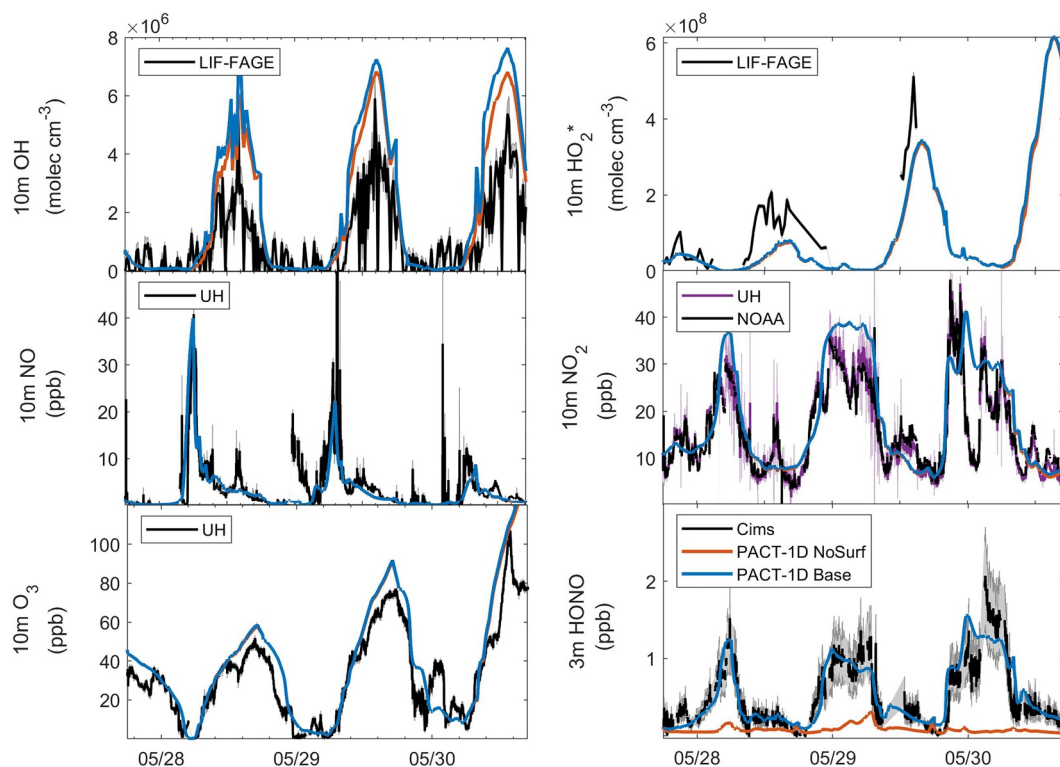


Figure 3. Overview plot showing NoSurf (orange) and Base (blue) model results compared to observations from May 27, 2010 18:00 through May 30, 2010 18:00. Measurement details are included in Table 1. HO_2^* is $\text{HO}_2 + 0.3\text{RO}_2$, following Griffith et al. (2016).

ppb. Modeled HONO does not capture the early morning peaks around 6:00–7:00 on May 29 and 30. This and the delayed decrease in HONO during the morning of May 30 indicate that the morning mixing may not be completely accurate in the model. A delay in morning boundary layer growth can prevent HONO formed overnight from mixing away from the surface. The quick changes in observed O_3 , NO_2 , and NO also indicate that there are air mass changes that the model cannot capture. Overall, these results show very good agreement between model and observations and show that a heterogeneous HONO surface source is necessary to simulate realistic atmospheric HONO levels. The mechanisms implemented here appropriately describe this heterogeneous source during CalNex.

4.3. HONO Vertical Profiles

Since HONO photolyzes quickly during transport away from the ground where it is formed, vertical profiles must be considered to understand HONO's sources and its total impact to air quality in the boundary layer. Observed profiles were constructed by vertically interpolating between the NOAA CIMS measurements at 3 m and the LP-DOAS measurements at 55.5 m, 99.5 m, 188 m, and 405.5 m. The CIMS and LP-DOAS instruments showed excellent agreement in another field experiment (UBWOS 2012). We are therefore confident that the two datasets can be combined to construct vertical concentration profiles of HONO. Figure 4 shows the observed profiles compared to PACT-1D for the entire three day period and Figure 5 shows select hours between May 27 18:00 and May 28 17:00.

In the observed profiles, the highest HONO concentrations are typically at the surface, which is consistent with vertical profiles measured in other field campaigns (Kleffmann et al., 2003; Tsai et al., 2018; Vandenberg et al., 2013; Villena et al., 2011; Wong et al., 2011, 2012; Young et al., 2012). The quick decay in HONO with altitude in the lowest 100 m, especially during the day, emphasizes the importance of vertical profile measurements and modeling. HONO's role in boundary layer chemistry can easily be over or under estimated if measurements at a single altitude are used. In particular, this can have a significant impact on OH

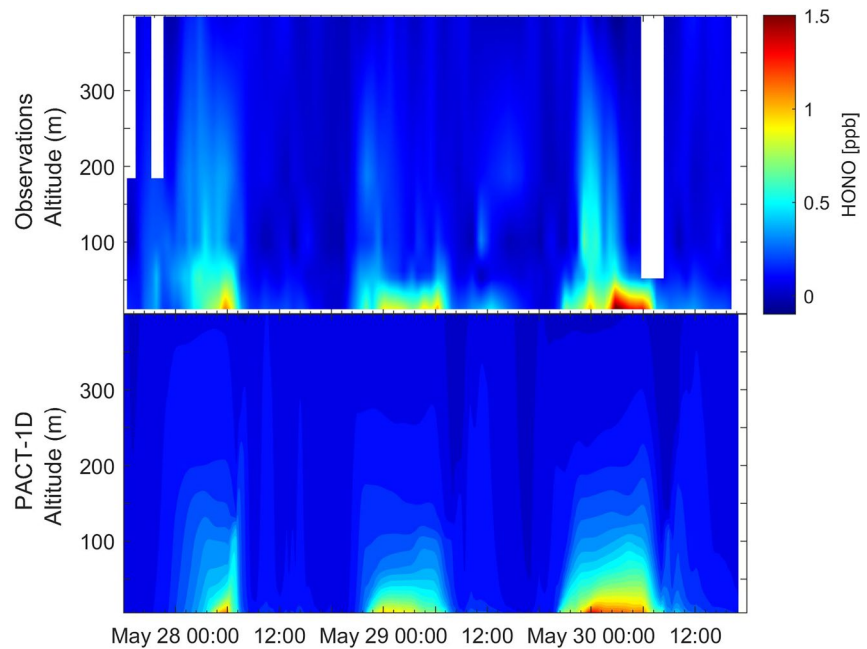


Figure 4. Comparison of HONO vertical concentration profiles between observations (top) and model (bottom), from May 27 18:00 to May 30 17:00. The observed profile is constructed from LP-DOAS data and NOAA CIMS data.

production rates, which will be discussed in the following section. Similar to other studies, we conclude that these profiles provide evidence for a ground source of HONO. The underestimation of HONO in the NoSurf run (Figure 5, right), shows that direct emissions cannot be the primary ground source. Accurately

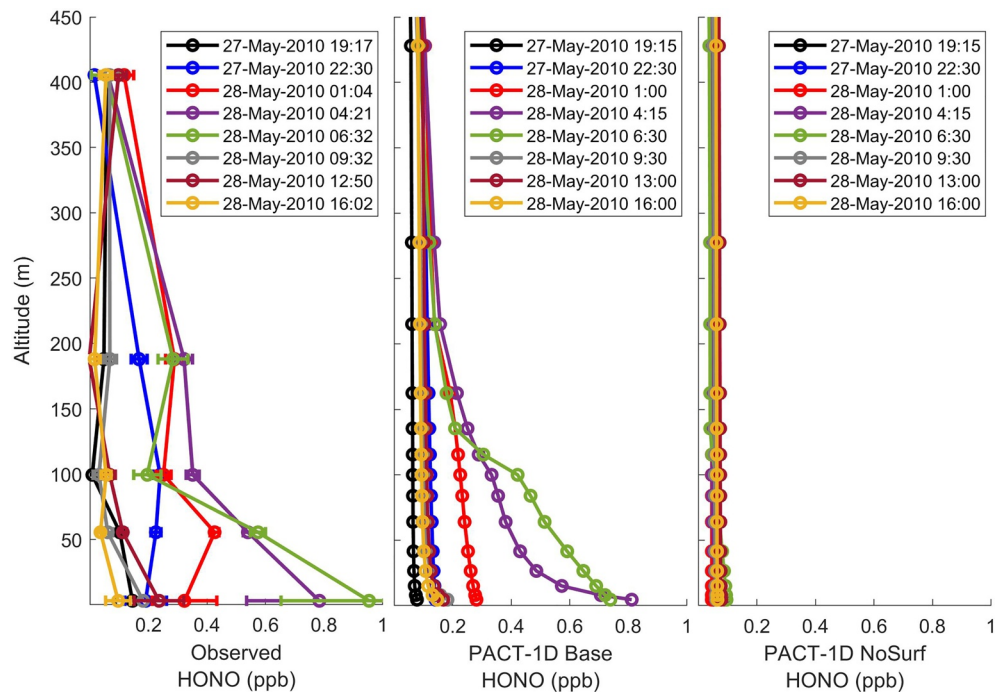


Figure 5. Comparison of HONO vertical concentration profiles between observations and model from May 27 to 28. The left panel is the observed profile, the middle is the PACT-1D Base run including surface chemistry, and the right panel is the PACT-1D NoSurf run excluding surface chemistry. The observed profile is constructed from LP-DOAS data (top four data points) and NOAA CIMS data (lowest data point).

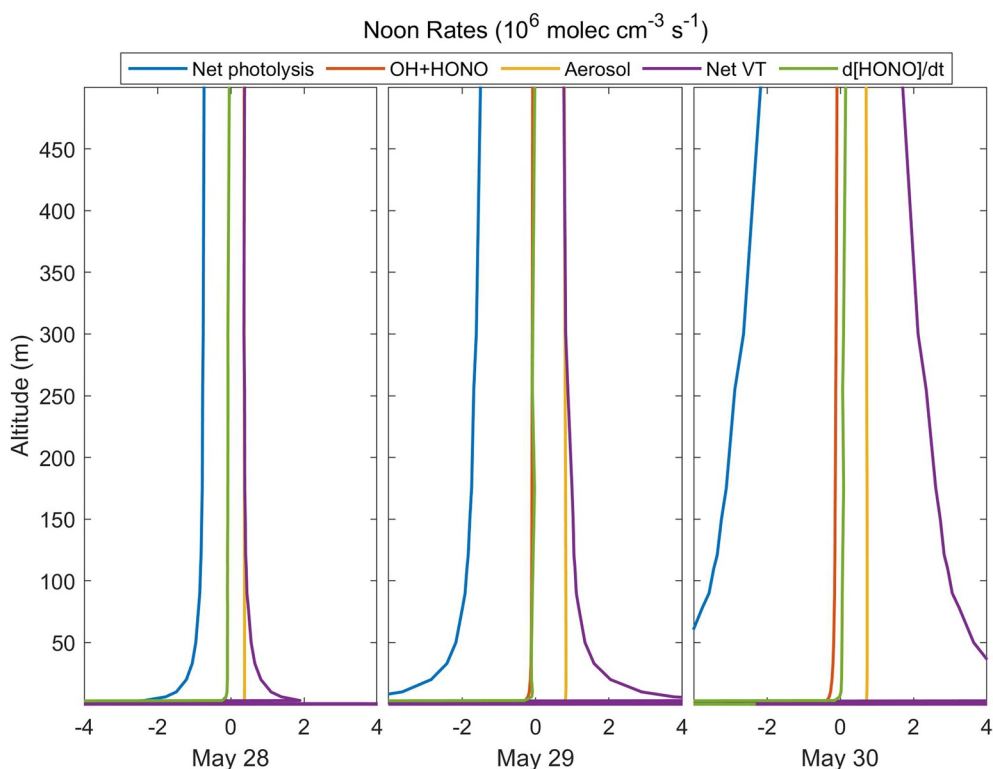


Figure 6. Noon time HONO budget for May 28 (left), 29 (middle), and 30 (right) from the Base run. Rates are reported in molecules $\text{cm}^{-3} \text{s}^{-1}$ and include net photolysis (HONO photolysis minus formation from the OH + NO reaction), loss via the HONO + OH reaction, formation from aerosol nitrate photolysis, net vertical transport, and the HONO concentration change with time.

implementing the heterogeneous HONO surface sources allowed us to better model HONO both near the surface and at higher altitudes.

The underestimation of HONO in the NoSurf run (Figure 5, right), which includes heterogeneous HONO formation from aerosol nitrate only, also shows that aerosol sources of HONO are less significant than ground sources. The aerosol source shows a diurnal trend, peaking in the early afternoon and decreasing to zero at night. In the Base run, the source peaks near 7×10^5 molecules $\text{cm}^{-3} \text{s}^{-1}$ on May 28, 9×10^5 on May 29, and 8×10^5 on May 30, within the LP-DOAS altitude range (50–400 m). Lower values on May 28 are due to smaller photolysis rates and lower aerosol number concentrations that day. Aerosol nitrate concentrations are under predicted compared to observations on this day as well so the values reported by our model are likely too low. On May 29, modeled aerosol nitrate concentrations are slightly higher than observed, indicating that the HONO aerosol source may be slightly over predicted as well. The values we report are generally consistent with other studies in urban areas, including Wong et al. (2013) who reports noontime values of $1.0\text{--}1.7 \times 10^6$ molecules $\text{cm}^{-3} \text{s}^{-1}$ in Houston, Texas. Our values are lower than those reported in more polluted cities with larger available aerosol surface area. Liu et al. (2021), for example, found approximately 1 ppb hr^{-1} (6.9×10^6 molecules $\text{cm}^{-3} \text{s}^{-1}$) of HONO could be formed from aerosol sources at noon in Beijing in summer. The higher rates in Beijing are likely due to the higher aerosol loading in that study.

Net vertical transport rates of HONO from below are more variable from day-to-day but, in general, are greater than or about equal to HONO production from aerosol nitrate. For most of the three day period, the primary source of HONO below 500 m is upward transport from the surface (Figure 6). The large difference in surface area between aerosols and the ground can explain the greater importance of ground sources and is in agreement with other studies (Kalberer et al., 1999; Kleffmann et al., 2003; Stemmler et al., 2007; Vogel et al., 2003). Compared to observations, daytime HONO levels between 50 m and 400 m in the Base run tend to be over predicted. This may indicate that the sources aloft (formation on aerosols and transport from

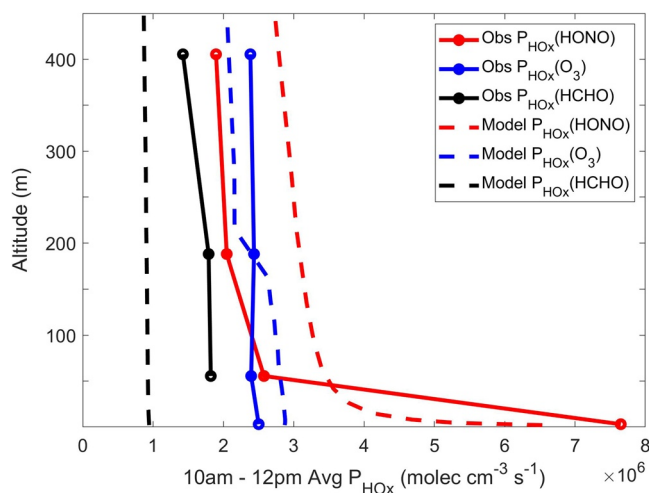


Figure 7. Primary HO_x production due to HONO (red), O₃ (blue), and HCHO (black). Observations are shown as dotted lines and model data from the Base run is shown as solid lines. Values are averaged between 10:00 a.m. and 12:00 p.m. on May 28, 2010.

below) are too high. There is uncertainty in the photolysis rate for the aerosol source in the model, and the vertical transport from the ground. Consequently, it is currently unclear which process is responsible for the disagreement.

4.4. Primary HO_x Production

To determine the importance of HONO to the radical budget, primary HO_x production (P_{HOx}) was calculated for the Base run and measurements. We considered three major primary HO_x production pathways, HONO photolysis, HCHO photolysis, and O₃ photolysis followed by reaction of O(¹D) with H₂O. Since HONO levels change quickly with altitude, as seen in the previous section, we again used vertical profiles to calculate P_{HOx} . In addition to HONO measurements, the LP-DOAS observed vertical profiles of HCHO and O₃. These were combined with the 3 m CIMS measurements of HONO, and the University of Houston's (UH) 10 m O₃ measurements to construct concentration profiles. 10m measurements of photolysis rates, temperature, and relative humidity (Table 1) were used to calculate P_{HOx} , assuming the values are constant over the altitude range considered here (0–450 m). Figure 7 shows vertical profiles of P_{HOx} from observations (solid lines) and model (dashed lines). These values are averages from 10:00 a.m. to 12:00 p.m. on May 28, 2010.

In both PACT-1D and observations, the contribution to P_{HOx} from HCHO and O₃ remains relatively constant with height, with higher values for O₃. PACT-1D underestimates P_{HOx} from HCHO compared to the observations, but captures the O₃ contribution well. Comparing HCHO LP-DOAS measurements to the model shows that PACT-1D under predicts HCHO levels at these altitudes, which leads to the under prediction of $P_{\text{HOx}}(\text{HCHO})$.

Both observations and PACT-1D show that HONO photolysis is dominant near the surface, contributing 2–3 times more than O₃ below 10 m. $P_{\text{HOx}}(\text{HONO})$ decreases quickly moving away from the surface, following the trend seen in the HONO concentration profile. PACT-1D underestimates $P_{\text{HOx}}(\text{HONO})$ compared to the observations at the surface by about 15% compared to observations, and over predicts at higher altitudes by 25%–35%. The model also underestimates HONO concentrations at the surface and over predicts them aloft during this time period (Figure 5) which can explain this difference in $P_{\text{HOx}}(\text{HONO})$. The discrepancy between model and observations, for both the concentration and $P_{\text{HOx}}(\text{HONO})$, is likely due to the high sensitivity of HONO to the vertical mixing or an over prediction of the HONO aerosol source, as discussed above.

A study by Griffith et al. (2016) found that during the CalNex campaign, HONO photolysis contributed 26% to the total radical production rate on weekends and holidays and 29% on weekdays. Using these average values, their $P_{\text{HOx}}(\text{HONO})$ between 10:00 a.m. and 12:00 p.m. ranged from about 5×10^6 and 8×10^6 molecules $\text{cm}^{-3} \text{s}^{-1}$. They note that these values are most appropriate for 10 m altitude where measurements were recorded, and are consistent with the values we report here at low altitudes. HCHO photolysis contributed 9%–10% to the total radical production, giving rates between 1.5×10^6 and 3×10^6 molecules $\text{cm}^{-3} \text{s}^{-1}$. The observations reported here are in agreement with these values, but again PACT-1D under predicts $P_{\text{HOx}}(\text{HCHO})$ due to the HCHO concentration being too low. O₃ photolysis contributed 11%–14%, with rates of 2×10^6 – 4.5×10^6 molecules $\text{cm}^{-3} \text{s}^{-1}$, matching our values well.

4.5. HONO Source Mechanisms

The HONO surface formation mechanisms added to PACT-1D in the Base run provided an additional source of up to 2.5×10^{11} molecules $\text{cm}^{-2} \text{s}^{-1}$ during the day and up to 5×10^{10} molecules $\text{cm}^{-2} \text{s}^{-1}$ during the night. Figure 8 shows the source rate for our three day period, including the contributions from individual mechanisms. Values remained relatively constant throughout each of the nights around 1×10^{10} to 5×10^{10} molecules $\text{cm}^{-2} \text{s}^{-1}$ and then increased quickly in the early morning as photolytic formation mechanisms become effective. Our values are higher than source rates reported by other field studies, which

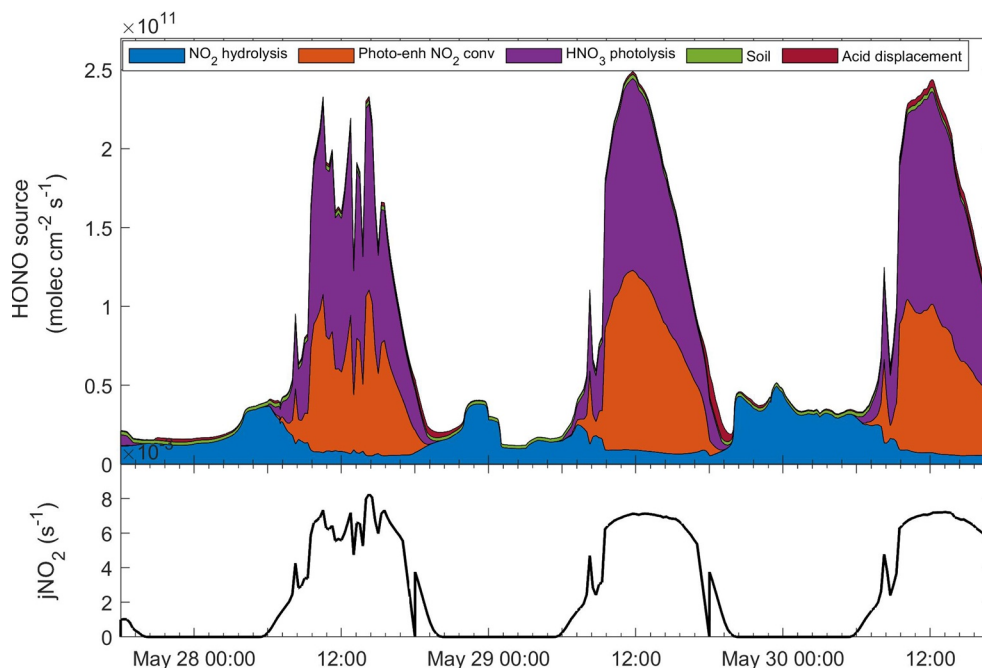


Figure 8. Contribution of individual mechanisms to the total HONO surface source in the Base run, from May 27, 2010 18:00 through May 30, 2010 17:00. The 10 m NO_2 photolysis rate for the three-day period is shown in the lower panel.

include a forest canopy (Zhang et al., 2009; Zheng et al., 2011), an agricultural site (Ren et al., 2011), and polluted rural site (Tsai et al., 2018). These studies report average noontime fluxes between 1×10^{10} and 3×10^{10} molecules $\text{cm}^{-2} \text{s}^{-1}$, measured at 10–20 m altitudes. Our surface flux is provided directly at the ground which likely explains the higher values. Loss of HONO through photolysis or deposition back to the ground decreases the amount that is transported to higher altitudes. We calculated the flux of HONO across 10 m in the model and found noontime values of 5×10^{10} molecules $\text{cm}^{-2} \text{s}^{-1}$ for May 28 and 29 and 1.1×10^{11} molecules $\text{cm}^{-2} \text{s}^{-1}$ for May 30. These are in better agreement with previous studies. Our urban site likely has a higher HONO source due to higher NO_2 concentrations and deposition, and higher surface HNO_3 concentrations.

The night time source was dominated by hydrolysis of NO_2 , which is consistent with previous studies (Kleffmann et al., 2003; VandenBoer et al., 2013; Wong et al., 2011). Photolysis of surface HNO_3 dominated throughout the day, contributing 45%–60% of the total source during mid-day. Photo-enhanced conversion of NO_2 was also significant, contributing 20%–45% of the daytime source (Figure 8).

Previous studies have suggested that the photo-enhanced conversion of NO_2 is the dominant heterogeneous mechanism under high- NO_x urban conditions while the photolysis of surface HNO_3 is more important under low- NO_x conditions (Elshorbany et al., 2012; Zhou et al., 2003). We find the opposite during CalNex. Pusede et al. (2015) examined how HONO levels during the CalNex campaign changed compared to NO_x and found daytime HONO production did not vary with weekday/weekend changes in NO_2 . They suggested therefore that NO_2 conversion is not the dominant HONO formation pathway. Although HNO_3 can also show a dependence on NO_x levels, its deposition and subsequent photolysis occur on a longer time scale which would not necessarily correlate with atmospheric NO_2 levels. Baergen and Donaldson (2016) suggests that HNO_3 photolysis on urban grime and its dependence on relative humidity would also cause a discrepancy between NO_2 and HONO production. Our results therefore support the findings by Pusede et al. (2015).

It is currently unclear, however, why these differ from the study performed by Wong et al. (2013) in Houston, Texas. They found that photo-enhanced NO_2 conversion was the dominant HONO source based on a clear correlation between HONO and NO_2 levels. It is possible that surface $\text{HNO}_3/\text{NO}_3^-$ concentrations

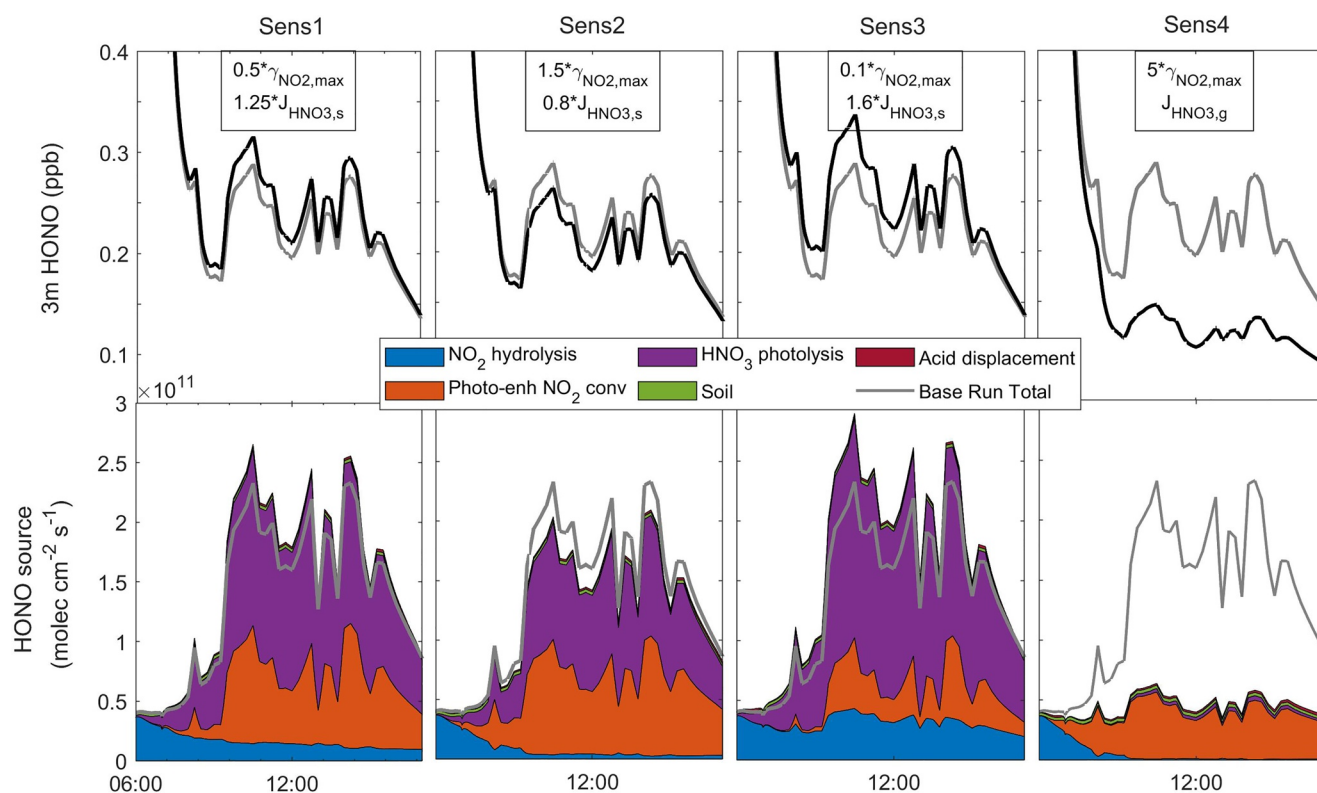


Figure 9. Results from sensitivity studies, showing 3 m HONO (top, black line) and the HONO ground source (bottom) for the afternoon of May 28. The Base run is shown in gray.

are higher in Los Angeles, giving more importance to its photolytic source. The scarcity of significant rain events in Southern California may cause a buildup of HNO_3 on surfaces, whereas the much more frequent precipitation in Houston can lead to surface adsorbed species being washed away. Guo et al. (2017) did find that particle nitrate and HNO_3 concentrations during CalNex were higher than measurements from summertime campaigns in the southeast United States. They suggest this is due to the higher NO_x versus SO_2 sources in southern California. This leads to a higher NO_3^- to SO_4^{2-} ratio in particles, which raises the pH. The higher pH then creates a positive feedback which forms more NO_3^- . Although Guo et al. (2017) focused on particles, it is possible that similar chemistry is occurring at the ground as well. Our results show that HNO_3 photolysis should be considered as an important HONO source in certain urban areas and may be especially important in regions with low precipitation and high NO_x emissions.

4.6. Source Sensitivity to Uptake Coefficient and Photolysis Rate

We performed sensitivity tests to better understand how the daytime HONO surface source is impacted by uncertainties in the mechanisms. The goal for these tests was to determine if the balance between the two major daytime mechanisms, the photo-enhanced conversion of NO_2 and the photolysis of surface HNO_3 , could be adjusted and still provide a sufficient HONO source to match observations. We focused on uncertainties in the maximum reactive uptake coefficient ($\gamma_{\text{NO}_2,\text{max}}$) and the photolysis rate enhancement of surface HNO_3 ($J_{\text{HNO}_3,\text{surf}}$) compared to the gas phase. Results from the sensitivity tests (Figure 9) are compared to the Base model run and a description of the changes made for each test are included in Table 2.

- Sens1—To address the impact of uncertainties in $\gamma_{\text{NO}_2,\text{max}}$, its value was reduced by 50% in Sens1. A corresponding increase in $J_{\text{HNO}_3,\text{surf}}$ by 25% was then needed to maintain a surface source similar to the Base run. The noontime surface source increased from 1.6×10^{11} in the Base run to 1.9×10^{11} molecules $\text{cm}^{-2} \text{s}^{-1}$ in Sens1. The contribution of photo-enhanced NO_2 conversion at noon decreased from

32% of the total source in the Base run to 26%. The contribution from surface HNO₃ photolysis increased from 60% in the Base to 65%.

- Sens2—Doubling $\gamma_{\text{NO}_2, \text{max}}$ required reducing $J_{\text{HNO}_3, \text{surf}}$ by 20% to maintain a surface source consistent with the Base run. This run again led to good agreement with the Base run, with the total source decreasing slightly to 1.5×10^{11} molecules cm⁻² s⁻¹. The contribution of photo-enhanced NO₂ conversion at noon increased to 39% and the contribution from surface HNO₃ photolysis decreased slightly to 58%.
- Sens3—Reducing $\gamma_{\text{NO}_2, \text{max}}$ by 90% and increasing $J_{\text{HNO}_3, \text{surf}}$ by 60% caused the 3 m HONO concentration and the total HONO source to become slightly higher. The concentration is still within the margin of error of the HONO CIMS measurements.
- Sens4—To test if the photo-enhanced NO₂ conversion could contribute the majority of the ground HONO source, $\gamma_{\text{NO}_2, \text{max}}$ was increased by a factor of 5 and $J_{\text{HNO}_3, \text{surf}}$ was set equal to $J_{\text{HNO}_3, \text{g}}$. This test clearly failed to produce a strong enough source to describe HONO concentrations at 3 m. It is evident therefore that surface HNO₃ photolysis is an essential contributor to the HONO source and that it needs to proceed at a faster rate than gas phase HNO₃ photolysis. It is also interesting that the photo-enhanced NO₂ source is lower here than in Sens2 at most times throughout the day. Increasing $\gamma_{\text{NO}_2, \text{max}}$ between the Base run and Sens2 caused an increase in the source due to greater NO₂ uptake and conversion but this trend obviously does not continue as $\gamma_{\text{NO}_2, \text{max}}$ is increased more. The NO₂ concentration in the lowest model layer in Sens4 is less than half the concentration in Sens2, indicating that the mechanism becomes transport limited. Although NO₂ is converted at a greater rate, this is depleting NO₂ near the surface that cannot be replenished quickly enough from aloft, leading to an overall decrease in HONO production.

Since both photolytic mechanisms have similar dependencies, including irradiance and NO_x concentrations, it can be difficult to determine which is more important for HONO production. These sensitivity tests show that the contributions from each mechanism are uncertain due to poorly constrained $\gamma_{\text{NO}_2, \text{max}}$ and $J_{\text{HNO}_3, \text{surf}}$. While it is possible for surface HNO₃ photolysis to explain most of the HONO source, NO₂ conversion alone cannot produce enough HONO in our case. Without additional laboratory studies that demonstrate the specific importance of each of these two mechanisms, it is clear that both can be considered important HONO sources in urban regions.

5. Conclusion

HONO's impact on secondary pollutant formation makes it an important species in urban environments. Since its heterogeneous formation mechanisms are poorly understood, we have developed a new one-dimensional chemistry and transport model, PACT-1D, to perform mechanistic studies that can help constrain the HONO budget. In particular, PACT-1D has the ability to do molecular level surface chemistry and emissions. The model has been tested against observations from the CalNex field campaign, which was performed in the urban region of Los Angeles. Multiple heterogeneous source mechanisms at the ground were added to the model which helped better simulate atmospheric HONO levels, both at the ground and throughout the boundary layer. We determined that the daytime HONO source was dominated by HNO₃/nitrate photolysis at the ground, followed by photo-enhanced conversion of NO₂. At night, the major HONO source was conversion of NO₂ on the ground. With these sources implemented we determined that HONO photolysis is the dominant contributor to primary OH production near the surface. This contribution decreases quickly with altitude, showing a similar vertical profile to HONO concentrations. These results emphasize the importance of atmospheric mixing when considering HONO's total impact to the boundary layer and help better understand the HONO sources in urban environments. Tests were also performed to determine the sensitivity of the two major daytime HONO sources to uncertainties in their mechanisms. While their relative contributions vary with the uncertainties, it's clear that both HNO₃/nitrate photolysis and photo-enhanced conversion of NO₂ should be considered to simulate HONO in urban atmospheres.

Data Availability Statement

The PACT-1D model code used in this study is available at <http://doi.org/10.5281/zenodo.4776419>. Output files for the base run used in this study are available at: <https://doi.org/10.5281/zenodo.4776977>. The CalNex data set is available at <https://www.esrl.noaa.gov/csd/projects/calnex/>.

Acknowledgments

This work was supported by the National Oceanic Atmospheric Administration's Atmospheric Chemistry, Climate and Carbon Cycle program. The authors acknowledge Amélie Klein and François Ravetta for their contributions to the PACT-1D model and Jessica Gilman for the VOC measurements used in the analysis. The authors would also like to thank Steve Brown (NOAA) for his valuable insights.

References

- Acker, K., Febo, A., Trick, S., Perrino, C., Bruno, P., Wiesen, P., et al. (2006). Nitrous acid in the urban area of Rome. *Atmospheric Environment*, 40(17), 3123–3133. <https://doi.org/10.1016/j.atmosenv.2006.01.028>
- Alicke, B., Geyer, A., Hofzumahaus, A., Holland, F., Konrad, S., Patz, H., & Platt, U. (2003). OH formation by HONO photolysis during the BERLIOZ experiment. *Journal of Geophysical Research*, 108(D4), 8247. <https://doi.org/10.1029/2001JD000579>
- Alicke, B., Platt, U., & Stutz, J. (2002). Impact of nitrous acid photolysis on the total hydroxyl radical budget during the Limitation of Oxidant Production/Pianura Padana Produzione di Ozono study in Milan. *Journal of Geophysical Research*, 107(D22), 8196. <https://doi.org/10.1029/2000JD000075>
- Ammann, M., Kalberer, M., Jost, D., Tobler, L., Rössler, E., Piguet, D., et al. (1998). Heterogeneous production of nitrous acid on soot in polluted air masses. *Nature*, 395(6698), 157–160. <https://doi.org/10.1038/25965>
- Aubin, D. G., & Abbatt, J. P. D. (2007). Interaction of NO₂ with hydrocarbon soot: Focus on HONO yield, surface modification, and mechanism. *Journal of Physical Chemistry A*, 111(28), 6263–6273. <https://doi.org/10.1021/jp068884h>
- Baergen, A. M., & Donaldson, D. J. (2013). Photochemical renoxification of nitric acid on real urban grime. *Environmental Science & Technology*, 47, 815–820. <https://doi.org/10.1021/es3037862>
- Baergen, A. M., & Donaldson, D. J. (2016). Formation of reactive nitrogen oxides from urban grime photochemistry. *Atmospheric Chemistry and Physics*, 16, 6355–6363. <https://doi.org/10.5194/acp-16-6355-2016>
- Bartels-Rausch, T., Brigante, M., Elshorbany, Y. F., Ammann, M., D'Anna, B., George, C., et al. (2010). Humic acid in ice: Photo-enhanced conversion of nitrogen dioxide into nitrous acid. *Atmospheric Environment*, 25(40), 5443–5450. <https://doi.org/10.1016/j.atmosenv.2009.12.025>
- Borbon, A., Gilman, J. B., Kuster, W. C., Grand, N., Chevallier, S., Colomb, A., et al. (2013). Emission ratios of anthropogenic volatile organic compounds in northern mid-latitude megacities: Observations versus emission inventories in Los Angeles and Paris. *Journal of Geophysical Research Atmospheres*, 118(4), 2041–2057. <https://doi.org/10.1002/jgrd.50059>
- Boy, M., Sogachev, A., Lauros, J., Zhou, L., Guenther, A., & Smolander, S. (2011). SOSA—A new model to simulate the concentrations of organic vapors and sulfuric acid inside the ABL—Part 1: Model description and initial evaluation. *Atmospheric Chemistry and Physics*, 11(1), 43–51. <https://doi.org/10.5194/acp-11-43-2011>
- Brasseur, G. P., & Jacob, D. J. (2017). *Modeling of atmospheric chemistry*. Cambridge University Press. <https://doi.org/10.1017/9781316544754>
- Brigante, M., Cazor, D., D'Anna, B., George, C., & Donaldson, D. J. (2008). Photoenhanced uptake of NO₂ by pyrene solid films. *Journal of Physical Chemistry A*, 112(39), 9503–9508. <https://doi.org/10.1021/jp802324g>
- Cao, L., Platt, U., & Gutheil, E. (2016). Role of the boundary layer in the occurrence and termination of the tropospheric ozone depletion events in polar spring. *Atmospheric Environment*, 132, 98–110. <https://doi.org/10.1016/j.atmosenv.2016.02.034>
- Cao, L., Sihler, H., Platt, U., & Gutheil, E. (2014). Numerical analysis of the chemical kinetic mechanisms of ozone depletion and halogen release in the polar troposphere. *Atmospheric Chemistry and Physics*, 14(7), 3771–3787. <https://doi.org/10.5194/acp-14-3771-2014>
- Czader, B. H., Rappenglück, B., Percell, P., Byun, D. W., Ngan, F., & Kim, S. (2012). Modeling nitrous acid and its impact on ozone and hydroxyl radical during the Texas Air Quality Study 2006. *Atmospheric Chemistry and Physics*, 12(15), 6939–6951. <https://doi.org/10.5194/acp-12-6939-2012>
- Dusanter, S., Vimal, D., Stevens, P. S., Volkamer, R., & Molina, L. T. (2009). Measurements of OH and HO₂ concentrations during the MCMA-2006 field campaign—Part 1: Deployment of the Indiana University laser-induced fluorescence instrument. *Atmospheric Chemistry and Physics*, 9(5), 1665–1685. <https://doi.org/10.5194/acp-9-1665-2009>
- Elshorbany, Y. F., Kurtenbach, R., Wiesen, P., Lissi, E., Rubio, M., Villena, G., et al. (2009). Oxidation capacity of the city air of Santiago, Chile. *Atmospheric Chemistry and Physics*, 9(3), 2257–2273. <https://doi.org/10.5194/acp-9-2257-2009>
- Elshorbany, Y. F., Steil, B., Brühl, C., & Lelieveld, J. (2012). Impact of HONO on global atmospheric chemistry calculated with an empirical parameterization in the EMAC model. *Atmospheric Chemistry and Physics Discussions*, 12(5), 12885–12934. <https://doi.org/10.5194/acpd-12-12885-2012>
- Fu, X., Wang, T., Zhang, L., Li, Q., Wang, Z., Xia, M., et al. (2019). The significant contribution of HONO to secondary pollutants during a severe winter pollution event in southern China. *Atmospheric Chemistry and Physics*, 19(1), 1–14. <https://doi.org/10.5194/acp-19-1-2019>
- Fuchs, N., & Sutugin, A. (1971). High-dispersed aerosols. In *Topics in current aerosol research*. Elsevier.
- George, C., Strekowski, R. S., Kleffmann, J., Stemmler, K., & Ammann, M. (2005). Photoenhanced uptake of gaseous NO₂ on solid organic compounds: A photochemical source of HONO? *Faraday Discussions*, 130(2), 195–210. <https://doi.org/10.1039/b417888m>
- Geyer, A., & Stutz, J. (2004a). Vertical profiles of NO₃, N₂O₅, O₃, and NO_x in the nocturnal boundary layer: 2. Model studies on the altitude dependence of composition and chemistry. *Journal of Geophysical Research*, 109(D12), 1–18. <https://doi.org/10.1029/2003JD004211>
- Geyer, A., & Stutz, J. (2004b). The vertical structure of OH-HO₂-RO₂ chemistry in the nocturnal boundary layer: A one-dimensional model study. *Journal of Geophysical Research*, 109(D16), 1–17. <https://doi.org/10.1029/2003JD004425>
- Gilman, J. B., Burkhardt, J. F., Lerner, B. M., Williams, E. J., Kuster, W. C., Goldan, P. D., et al. (2010). Ozone variability and halogen oxidation within the Arctic and sub-Arctic springtime boundary layer. *Atmospheric Chemistry and Physics*, 10(21), 10223–10236. <https://doi.org/10.5194/acp-10-10223-2010>
- Goliff, W. S., Stockwell, W. R., & Lawson, C. V. (2013). The regional atmospheric chemistry mechanism, version 2. *Atmospheric Environment*, 68, 174–185. <https://doi.org/10.1016/j.atmosenv.2012.11.038>
- Granier, C., Darras, S., Denier Van Der Gon, H., Jana, D., Elguindi, N., Bo, G., & Kuenen, J. (2019). *The Copernicus Atmosphere Monitoring Service global and regional emissions (April 2019 version)*. Data from ECCAD.
- Griffith, S. M., Hansen, R., Dusanter, S., Michoud, V., Gilman, J., Kuster, W., et al. (2016). Measurements of hydroxyl and hydroperoxy radicals during CalNex-LA: Model comparisons and radical budgets. *Journal of Geophysical Research : Atmospheres*, 121, 4211–4232. <https://doi.org/10.1002/2015JD024358>

- Guo, H., Liu, J., Froyd, K. D., Roberts, J. M., Veres, P. R., Hayes, P. L., et al. (2017). Fine particle pH and gas-particle phase partitioning of inorganic species in Pasadena, California, during the 2010 CalNex campaign. *Atmospheric Chemistry and Physics*, 17(9), 5703–5719. <https://doi.org/10.5194/acp-17-5703-2017>
- Gutzwiller, L., Arens, F., Baltensperger, U., Gaggeler, H., & Ammann, M. (2002). Significance of semivolatiles diesel exhaust organics for secondary HONO formation. *Environmental Science and Technology*, 36(4), 677–682. <https://doi.org/10.1021/es015673b>
- Hayes, P. L., Ortega, A. M., Cubison, M. J., Froyd, K. D., Zhao, Y., Cliff, S. S., et al. (2013). Organic aerosol composition and sources in Pasadena, California, during the 2010 CalNex campaign. *Journal of Geophysical Research Atmospheres*, 118(16), 9233–9257. <https://doi.org/10.1002/jgrd.50530>
- Jenkin, M., Cox, R., & Williams, D. (1988). Laboratory studies of the kinetics of formation of nitrous acid from the thermal reaction of nitrogen dioxide and water vapor. *Atmospheric Environment*, 22(3), 487–498. [https://doi.org/10.1016/0004-6981\(88\)90194-1](https://doi.org/10.1016/0004-6981(88)90194-1)
- Kalberer, M., Ammann, M., Arens, F., Gaggeler, H. W., & Baltensperger, U. (1999). Heterogeneous formation of nitrous acid (HONO) on soot aerosol particles. *Journal of Geophysical Research*, 104, 13825–13832. <https://doi.org/10.1029/1999jd900141>
- Karamchandani, P., Emery, C., Yarwood, G., Lefer, B., Stutz, J., Couzo, E., & Vizuete, W. (2014). Implementation and refinement of a surface model for heterogeneous HONO formation in a 3-D chemical transport model. *Atmospheric Environment*, 112, 356–368. <https://doi.org/10.1016/j.atmosenv.2015.01.046>
- Khalizov, A. F., Cruz-Quinones, M., & Zhang, R. (2010). Heterogeneous reaction of NO₂ on fresh and coated soot surfaces. *Journal of Physical Chemistry A*, 114(28), 7516–7524. <https://doi.org/10.1021/jp1021938>
- Kim, S., McDonald, B. C., Baidar, S., Brown, S. S., Dube, B., Ferrare, R. A., et al. (2016). Modeling the weekly cycle of NO_x and CO emissions and their impacts on O₃ in the Los Angeles-South Coast Air Basin during the CalNex 2010 field campaign. *Journal of Geophysical Research: Atmospheres*, 121, 1340–1360. <https://doi.org/10.1002/2015JD024292>
- Kirchstetter, T. W., Harley, R. A., & Littlejohn, D. (1996). Measurement of nitrous acid in motor vehicle exhaust. *Environmental Science and Technology*, 30, 2843–2849. <https://doi.org/10.1021/es960135y>
- Kleffmann, J. (2007). Daytime sources of nitrous acid (HONO) in the atmospheric boundary layer. *ChemPhysChem*, 8(8), 1137–1144. <https://doi.org/10.1002/cphc.200700016>
- Kleffmann, J., Gavriloaiei, T., Hofzumahaus, A., Holland, F., Koppmann, R., Rupp, L., & Wahner, A. (2005). Daytime formation of nitrous acid: A major source of OH radicals in a forest. *Geophysical Research Letters*, 32, L05818. <https://doi.org/10.1029/2005GL022524>
- Kleffmann, J., Kurtenbach, R., Lörzer, J., Wiesen, P., Kalthoff, N., Vogel, B., & Vogel, H. (2003). Measured and simulated vertical profiles of nitrous acid - Part I: Field measurements. *Atmospheric Environment*, 37(21), 2949–2955. [https://doi.org/10.1016/S1352-2310\(03\)00242-5](https://doi.org/10.1016/S1352-2310(03)00242-5)
- Kleffmann, J., Lörzer, J. C., Wiesen, P., Kern, C., Trick, S., Volkamer, R., et al. (2006). Intercomparison of the DOAS and LOPAP techniques for the detection of nitrous acid (HONO). *Atmospheric Environment*, 40(20), 3640–3652. <https://doi.org/10.1016/j.atmosenv.2006.03.027>
- Kramer, L., Crilley, L., Adams, T., Ball, S., Pope, F., & Bloss, W. (2019). Nitrous acid (HONO) emissions under real-world driving conditions from vehicles in a UK road tunnel. *Atmospheric Chemistry and Physics*, 19(2), 1–31. <https://doi.org/10.5194/acp-2019-1070>
- Kurtenbach, R., Becker, K. H., Gomes, J. A. G., Kleffmann, J., Lörzer, J., Spittler, M., et al. (2001). Investigations of emissions and heterogeneous formation of HONO in a road traffic tunnel. *Atmospheric Environment*, 35, 3385–3394. [https://doi.org/10.1016/S1352-2310\(01\)00138-8](https://doi.org/10.1016/S1352-2310(01)00138-8)
- Lammel, G., & Cape, J. (1996). Nitrous acid and nitrite in the atmosphere. *Chemical Society Reviews*, 25, 361–369. <https://doi.org/10.1039/CS9962500361>
- Laufs, S., Cazaunau, M., Stella, P., Kurtenbach, R., Cellier, P., Mellouki, A., et al. (2017). Diurnal fluxes of HONO above a crop rotation. *Atmospheric Chemistry and Physics*, 17(11), 6907–6923. <https://doi.org/10.5194/acp-17-6907-2017>
- Li, Y., An, J., Min, M., Zhang, W., Wang, F., & Xie, P. (2011). Impacts of HONO sources on the air quality in Beijing, Tianjin and Hebei Province of China. *Atmospheric Environment*, 45(27), 4735–4744. <https://doi.org/10.1016/j.atmosenv.2011.04.086>
- Liu, J., Liu, Z., Ma, Z., Yang, S., Yao, D., Zhao, S., et al. (2021). Detailed budget analysis of HONO in Beijing, China: Implication on atmosphere oxidation capacity in polluted megacity. *Atmospheric Environment*, 244, 117957. <https://doi.org/10.1016/j.atmosenv.2020.117957>
- Maljanen, M., Yli-Pirilä, P., Hytönen, J., Joutsensaari, J., & Martikainen, P. J. (2013). Acidic northern soils as sources of atmospheric nitrous acid (HONO). *Soil Biology and Biochemistry*, 67(2), 94–97. <https://doi.org/10.1016/j.soilbio.2013.08.013>
- Mao, J., Ren, X., Chen, S., Brune, W. H., Chen, Z., Martinez, M., et al. (2010). Atmospheric oxidation capacity in the summer of Houston 2006: Comparison with summer measurements in other metropolitan studies. *Atmospheric Environment*, 44(33), 4107–4115. <https://doi.org/10.1016/j.atmosenv.2009.01.013>
- Meusel, H., Tamm, A., Kuhn, U., Wu, D., Lena Leifke, A., Fiedler, S., et al. (2018). Emission of nitrous acid from soil and biological soil crusts represents an important source of HONO in the remote atmosphere in Cyprus. *Atmospheric Chemistry and Physics*, 18(2), 799–813. <https://doi.org/10.5194/acp-18-799-2018>
- Monge, M. E., D'Anna, B., & George, C. (2010). Nitrogen dioxide removal and nitrous acid formation on titanium oxide surfaces—An air quality remediation process? *Physical Chemistry Chemical Physics*, 12(31), 8991–8998. <https://doi.org/10.1039/b925785c>
- Neuman, J. A., Ryerson, T. B., Huey, L. G., Jakoubek, R., Nowak, J. B., Simons, C., & Fehsenfeld, F. C. (2003). Calibration and evaluation of nitric acid and ammonia permeation tubes by UV optical absorption. *Environmental Science and Technology*, 37(13), 2975–2981. <https://doi.org/10.1021/es0264221>
- Neuman, J. A., Trainer, M., Brown, S. S., Min, K.-E., Nowak, J. B., Parrish, D. D., et al. (2016). HONO emission and production determined from airborne measurements over the Southeast U.S. *Journal of Geophysical Research*, 121(15), 9237–9250. <https://doi.org/10.1002/2016JD025197>
- Oswald, R., Behrendt, T., Ermel, M., Wu, D., Su, H., Cheng, Y., et al. (2013). HONO emissions from soil bacteria as a major source of atmospheric reactive nitrogen. *Science*, 341(6151), 1233–1235. <https://doi.org/10.1126/science.1242266>
- Pitts, J., Sanhueza, E., Atkinson, R., Carter, W., Winer, A., Harris, G. W., & Plum, C. (1984). An investigation of the dark formation of nitrous acid in environmental chambers. *International Journal of Chemical Kinetics*, 16, 919–939. <https://doi.org/10.1002/kin.550160712>
- Platt, U., & Stutz, J. (2008). *Differential optical absorption spectroscopy*. Springer Berlin Heidelberg. <https://doi.org/10.1007/978-3-540-75776-4>
- Pollack, I. B., Lerner, B. M., & Ryerson, T. B. (2010). Evaluation of ultraviolet light-emitting diodes for detection of atmospheric NO₂ by photolysis—Chemiluminescence. *Journal of Atmospheric Chemistry*, 65(2–3), 111–125. <https://doi.org/10.1007/s10874-011-9184-3>
- Pusede, S. E., VandenBoer, T. C., Murphy, J. G., Markovic, M. Z., Young, C. J., Veres, P. R., et al. (2015). An atmospheric constraint on the NO₂ dependence of daytime near-surface nitrous acid (HONO). *Environmental Science and Technology*, 49(21), 12774–12781. <https://doi.org/10.1021/acs.est.5b02511>
- Ramazan, K. A., Syomin, D., & Finlayson-Pitts, B. J. (2004). The photochemical production of HONO during the heterogeneous hydrolysis of NO₂. *Physical Chemistry Chemical Physics*, 6(14), 3836–3843. <https://doi.org/10.1039/b402195a>

- Ren, X., Harder, H., Martinez, M., & Leshner, R. (2003). HO₂ concentrations and OH reactivity observations in New York City during PMTACS-NY2001. *Atmospheric Environment*, 37(26), 3627–3637. [https://doi.org/10.1016/S1352-2310\(03\)00460-6](https://doi.org/10.1016/S1352-2310(03)00460-6)
- Ren, X., Sanders, J. E., Rajendran, A., Weber, R. J., Goldstein, A. H., Pusede, S. E., et al. (2011). A relaxed eddy accumulation system for measuring vertical fluxes of nitrous acid. *Atmospheric Measurement Techniques*, 4(10), 2093–2103. <https://doi.org/10.5194/amt-4-2093-2011>
- Roberts, J. M., Veres, P., Warneke, C., Neuman, J. A., Washenfelder, R. A., Brown, S. S., et al. (2010). Measurement of HONO, HNCO, and other inorganic acids by negative-ion proton-transfer chemical-ionization mass spectrometry (NI-PT-CIMS): Application to biomass burning emissions. *Atmospheric Measurement Techniques*, 3(4), 981–990. <https://doi.org/10.5194/amt-3-981-2010>
- Ryerson, T. B., Andrews, A. E., Angevine, W. M., Bates, T. S., Brock, C. A., Cairns, B., et al. (2013). The 2010 California Research at the Nexus of Air Quality and Climate Change (CalNex) field study. *Journal of Geophysical Research: Atmospheres*, 118(11), 5830–5866. <https://doi.org/10.1002/jgrd.50331>
- Sakamaki, F., Hatakeyama, S., & Akimoto, H. (1983). Formation of nitrous acid and nitric oxide in the heterogeneous dark reaction of nitrogen dioxide and water vapor in a smog chamber. *International Journal of Chemical Kinetics*, 15, 1013–1029. <https://doi.org/10.1002/kin.550151006>
- Sandu, A., & Sander, R. (2006). Technical note: Simulating chemical systems in Fortran90 and Matlab with the Kinetic PreProcessor KPP-2.1. *Atmospheric Chemistry and Physics*, 6(1), 187–195. <https://doi.org/10.5194/acp-6-187-2006>
- Sarwar, G., Roselle, S. J., Mathur, R., Appel, W., Dennis, R. L., & Vogel, B. (2008). A comparison of CMAQ HONO predictions with observations from the Northeast Oxidant and Particle Study. *Atmospheric Environment*, 42(23), 5760–5770. <https://doi.org/10.1016/j.atmosenv.2007.12.065>
- Scharko, N. K., Schütte, U. M. E., Berke, A. E., Banina, L., Peel, H. R., Donaldson, M. A., et al. (2015). Combined flux chamber and genomics approach links nitrous acid emissions to ammonia oxidizing bacteria and archaea in urban and agricultural soil. *Environmental Science & Technology*, 49(23), 13825–13834. <https://doi.org/10.1021/acs.est.5b00838>
- Shetter, R. E., & Müller, M. (1999). Photolysis frequency measurements using actinic flux spectroradiometry during the PEM-Tropics mission: Instrumentation description and some results. *Journal of Geophysical Research: Atmospheres*, 104(D5), 5647–5661. <https://doi.org/10.1029/98JD01381>
- Simpson, D., Andersson, C., Christensen, J. H., Engardt, M., Geels, C., Nyiri, A., et al. (2014). Impacts of climate and emission changes on nitrogen deposition in Europe: A multi-model study. *Atmospheric Chemistry and Physics*, 14(13), 6995–7017. <https://doi.org/10.5194/acp-14-6995-2014>
- Stemmler, K., Ammann, M., Donders, C., Kleffmann, J., & George, C. (2006). Photosensitized reduction of nitrogen dioxide on humic acid as a source of nitrous acid. *Nature*, 440(7081), 195–198. <https://doi.org/10.1038/nature04603>
- Stemmler, K., Ndour, M., Elshorbany, Y., Kleffmann, J., D'Anna, B., George, C., et al. (2007). Light induced conversion of nitrogen dioxide into nitrous acid on submicron humic acid aerosol. *Atmospheric Chemistry and Physics*, 7(16), 4237–4248. <https://doi.org/10.5194/acp-7-4237-2007>
- Stutz, J., Wong, K. W., Lawrence, L., Ziemba, L., Flynn, J. H., Rappenglück, B., & Lefer, B. (2010). Nocturnal NO₃ radical chemistry in Houston, TX. *Atmospheric Environment*, 44(33), 4099–4106. <https://doi.org/10.1016/j.atmosenv.2009.03.004>
- Su, H., Cheng, Y., Oswald, R., Behrendt, T., Trebs, I., Meixner, F. X., et al. (2011). Soil nitrite as a source of atmospheric HONO and OH radicals. *Science*, 333(6049), 1616–1618. <https://doi.org/10.1126/science.1207687>
- Svensson, R., Ljungström, E., & Lindqvist, O. (1987). Kinetics of the reaction between nitrogen dioxide and water vapor. *Atmospheric Environment*, 21(7), 1529–1539. [https://doi.org/10.1016/0004-6981\(87\)90315-5](https://doi.org/10.1016/0004-6981(87)90315-5)
- Thomas, J. L., Dibb, J. E., Huey, L. G., Liao, J., Tanner, D., Lefer, B., et al. (2012). Modeling chemistry in and above snow at Summit, Greenland – Part 2: Impact of snowpack chemistry on the oxidation capacity of the boundary layer. *Atmospheric Chemistry and Physics*, 12(14), 6537–6554. <https://doi.org/10.5194/acp-12-6537-2012>
- Thomas, J. L., Stutz, J., Lefer, B., Huey, L. G., Toyota, K., Dibb, J. E., & von Glasow, R. (2011). Modeling chemistry in and above snow at Summit, Greenland – Part 1: Model description and results. *Atmospheric Chemistry and Physics*, 11(10), 4899–4914. <https://doi.org/10.5194/acp-11-4899-2011>
- Toyota, K., Dastoor, A. P., & Ryzhkov, A. (2014). Air-snowpack exchange of bromine, ozone and mercury in the springtime Arctic simulated by the 1-D model PHANTAS—Part 2: Mercury and its speciation. *Atmospheric Chemistry and Physics*, 14(8), 4135–4167. <https://doi.org/10.5194/acp-14-4135-2014>
- Trick, S. (2004). *Formation of nitrous acid on urban surfaces—A physical chemical perspective* (Unpublished doctoral dissertation).
- Tsai, C., Spolaor, M., Fedele Colosimo, S., Pikelnaya, O., Cheung, R., Williams, E., et al. (2018). Nitrous acid formation in a snow-free wintertime polluted rural area. *Atmospheric Chemistry and Physics*, 18(3), 1977–1996. <https://doi.org/10.5194/acp-18-1977-2018>
- Tsai, C., Wong, C., Hurlock, S., Pikelnaya, O., Mielke, L. H., Osthoff, H. D., et al. (2014). Nocturnal loss of NO₃ during the 2010 CalNex-LA study in the Los Angeles Basin. *Journal of Geophysical Research*, 119(22), 13004–13013. <https://doi.org/10.1002/2014JD022171>
- VandenBoer, T. C., Brown, S. S., Murphy, J. G., Keene, W. C., Young, C. J., Pszenny, A. A. P., et al. (2013). Understanding the role of the ground surface in HONO vertical structure: High resolution vertical profiles during NACHTT-11. *Journal of Geophysical Research: Atmospheres*, 118, 10155–10171. <https://doi.org/10.1002/jgrd.50721>
- VandenBoer, T. C., Young, C. J., Talukdar, R. K., Markovic, M. Z., Brown, S. S., Roberts, J. M., & Murphy, J. G. (2015). Nocturnal loss and daytime source of nitrous acid through reactive uptake and displacement. *Nature Geoscience*, 8(1), 55–60. <https://doi.org/10.1038/ngeo2298>
- Veres, P. R., Roberts, J. M., Cochran, A. K., Gilman, J. B., Kuster, W. C., Holloway, J. S., et al. (2011). Evidence of rapid production of organic acids in an urban air mass. *Geophysical Research Letters*, 38(17). <https://doi.org/10.1029/2011GL048420>
- Veres, P. R., Roberts, J. M., Warneke, C., Welsh-Bon, D., Zahniser, M., Herndon, S., et al. (2008). Development of negative-ion proton-transfer chemical-ionization mass spectrometry (NI-PT-CIMS) for the measurement of gas-phase organic acids in the atmosphere. *International Journal of Mass Spectrometry*, 274(1–3), 48–55. <https://doi.org/10.1016/j.ijms.2008.04.032>
- Villena, G., Wiesen, P., Cantrell, C. A., Flocke, F., Fried, A., Hall, S. R., et al. (2011). Nitrous acid (HONO) during polar spring in Barrow, Alaska: A net source of OH radicals? *Journal of Geophysical Research*, 116, D00R07. <https://doi.org/10.1029/2011JD016643>
- Vogel, B., Vogel, H., Kleffmann, J., & Kurtenbach, R. (2003). Measured and simulated vertical profiles of nitrous acid—Part II. Model simulations and indications for a photolytic source. *Atmospheric Environment*, 37(21), 2957–2966. [https://doi.org/10.1016/S1352-2310\(03\)00243-7](https://doi.org/10.1016/S1352-2310(03)00243-7)
- Volkamer, R., Sheehy, P., Molina, L. T., & Molina, M. J. (2010). Oxidative capacity of the Mexico City atmosphere—Part 1: A radical source perspective. *Atmospheric Chemistry and Physics*, 10(14), 6969–6991. <https://doi.org/10.5194/acp-10-6969-2010>
- von Glasow, R., Sander, R., Bott, A., & Crutzen, P. J. (2002a). Modeling halogen chemistry in the marine boundary layer 1. Cloud-free MBL. *Journal of Geophysical Research*, 107(D17), ACH 9-1–ACH 9-16. <https://doi.org/10.1029/2001JD000942>

- von Glasow, R., Sander, R., Bott, A., & Crutzen, P. P. J. (2002b). Modeling halogen chemistry in the marine boundary layer 2. Interactions with sulfur and the cloud-covered MBL. *Journal of Geophysical Research*, *107*(D17), ACH 2-1-ACH 2-12. <https://doi.org/10.1029/2001JD000943>
- Wang, S., McNamara, S. M., Kolesar, K. R., May, N. W., Fuentes, J. D., Cook, R. D., et al. (2020). Urban snowpack ClNO₂ production and fate: A one-dimensional modeling study. *ACS Earth and Space Chemistry*, *4*(7), 1140–1148. <https://doi.org/10.1021/acsearthspacechem.0c00116>
- Washenfelder, R. A., Wagner, N. L., Dube, W. P., & Brown, S. S. (2011). Measurement of atmospheric ozone by cavity ring-down spectroscopy. *Environmental Science and Technology*, *45*(7), 2938–2944. <https://doi.org/10.1021/es103340u>
- Wolfe, G. M., Marvin, M. R., Roberts, S. J., Travis, K. R., & Liao, J. (2016). The framework for 0-D atmospheric modeling (F0AM) v3.1. *Geoscientific Model Development*, *9*(9), 3309–3319. <https://doi.org/10.5194/gmd-9-3309-2016>
- Wong, K., Oh, H.-J., Lefer, B. L., Rappenglück, B., & Stutz, J. (2011). Vertical profiles of nitrous acid in the nocturnal urban atmosphere of Houston, TX. *Atmospheric Chemistry and Physics*, *11*(8), 3595–3609. <https://doi.org/10.5194/acp-11-3595-2011>
- Wong, K., Tsai, C., Lefer, B., Grossberg, N., & Stutz, J. (2013). Modeling of daytime HONO vertical gradients during SHARP 2009. *Atmospheric Chemistry and Physics*, *13*(7), 3587–3601. <https://doi.org/10.5194/acp-13-3587-2013>
- Wong, K., Tsai, C., Lefer, B., Haman, C., Grossberg, N., Brune, W., et al. (2012). Daytime HONO vertical gradients during SHARP 2009 in Houston, TX. *Atmospheric Chemistry and Physics*, *12*(2), 635–652. <https://doi.org/10.5194/acp-12-635-2012>
- Ye, C., Gao, H., Zhang, N., & Zhou, X. (2016). Photolysis of nitric acid and nitrate on natural and artificial surfaces. *Environmental Science and Technology*, *50*(7), 3530–3536. <https://doi.org/10.1021/acs.est.5b05032>
- Ye, C., Zhang, N., Gao, H., & Zhou, X. (2019). Matrix effect on surface-catalyzed photolysis of nitric acid. *Scientific Reports*, *9*(1), 4351. <https://doi.org/10.1038/s41598-018-37973-x>
- Young, C. J., Washenfelder, R. A., Roberts, J. M., Mielke, L. H., Osthoff, H. D., Tsai, C., et al. (2012). Vertically resolved measurements of nighttime radical reservoirs in Los Angeles and their contribution to the urban radical budget. *Environmental Science & Technology*, *46*(20), 10965–10973. <https://doi.org/10.1021/es302206a>
- Zhang, N., Zhou, X., Bertman, S., Tang, D., Alaghmand, M., Shepson, P. B., & Carroll, M. A. (2012). Measurements of ambient HONO concentrations and vertical HONO flux above a northern Michigan forest canopy. *Atmospheric Chemistry and Physics Discussions*, *12*(3), 7273–7304. <https://doi.org/10.5194/acpd-12-7273-2012>
- Zhang, N., Zhou, X., Shepson, P. B., Gao, H., Alaghmand, M., & Stirm, B. (2009). Aircraft measurement of HONO vertical profiles over a forested region. *Geophysical Research Letters*, *36*(15), L15820. <https://doi.org/10.1029/2009GL038999>
- Zheng, W., Flocke, F. M., Tyndall, G. S., Swanson, A., Orlando, J. J., Roberts, J. M., et al. (2011). Characterization of a thermal decomposition chemical ionization mass spectrometer for the measurement of peroxy acyl nitrates (PANs) in the atmosphere. *Atmospheric Chemistry and Physics*, *11*(13), 6529–6547. <https://doi.org/10.5194/acp-11-6529-2011>
- Zhou, X., Civerolo, K., Dai, H., Huang, G., Schwab, J., & Demerjian, K. (2002). Summertime nitrous acid chemistry in the atmospheric boundary layer at a rural site in New York State. *Journal of Geophysical Research*, *107*(D21), ACH 13-1-ACH 13-11. <https://doi.org/10.1029/2001JD001539>
- Zhou, X., Gao, H., He, Y., Huang, G., Bertman, S., Civerolo, K., & Schwab, J. (2003). Nitric acid photolysis on surfaces in low-NO_x environments: Significant atmospheric implications. *Geophysical Research Letters*, *30*(23). <https://doi.org/10.1029/2003GL018620>
- Zhou, X., Huang, G., Civerolo, K., Roychowdhury, U., & Demerjian, K. L. (2007). Summertime observations of HONO, HCHO, and O₃ at the summit of Whiteface Mountain, New York. *Journal of Geophysical Research*, *112*, D08311. <https://doi.org/10.1029/2006JD007256>
- Zhou, X., Zhang, N., TerAvest, M., Tang, D., Hou, J., Bertman, S., et al. (2011). Nitric acid photolysis on forest canopy surface as a source for tropospheric nitrous acid. *Nature Geoscience*, *4*(6), 400–443. <https://doi.org/10.1038/ngeo1164>